been demonstrated that the ELN system is useful for further risk stratification of younger adult patients with CN-AML.[20,21] However, it has been reported that another genetic status, such as mutations in epigenetic modifier-encoding genes, could more precisely distinguish the prognosis in each ELN-risk group.[5,22] In addition, the prognostic impacts of recently identified mutations in spliceosome and cohesin complex genes on AML remain unclear.

The Japan Adult Leukemia Study Group (JALSG) conducted six phase III trials for adult *de novo* AML from 1987 (AML87, AML89, AML92, AML95, AML97 and AML201).[23] In the JALSG AML201 study, we prospectively compared a standard dose of idarubicin (IDR) with a higher dose of daunorubicin (HiDNR) in combination with cytarabine (Ara-C) as induction therapy, and three courses of high-dose Ara-C (HiDAC) with four courses of conventional standard-dose multiagents as consolidation therapy in CR patients.[24,25] We demonstrated that HiDNR was equivalent to IDR, as induction therapy and HiDAC was of benefit only to patients with core-binding factor (CBF)-AML as consolidation therapy. Although the CR rate remained at 75–80% during the six JALSG studies, 7-year overall survival (OS) was improved to 48% in the AML201 study from 29% in the AML87 study. Allo-SCT was conducted in only 7.1% of registered patients in the AML87 study, whereas 45.8% of registered patients received allo-SCT not only at the first CR but also after relapse or primary induction failure in the AML201 study, indicating that active application of allo-SCT even after relapse or primary induction failure might contribute to the improvement of OS. These results collectively suggested that a novel risk stratification system for decision making of allo-SCT at the first CR is required.

In this study, we comprehensively analyzed mutations in 51 genes that have been recurrently identified in myeloid neoplasm as well as cytogenetics, and evaluated the association of genetic status with prognostic and clinical features in patients who were registered in the AML201 study.

PATIENTS AND METHODS

Patients and samples

The study population included 197 newly diagnosed *de novo* AML patients, except for those with acute promyelocytic leukemia, who were registered in the JALSG AML201 study (UMIN Clinical Trials Registry C000000157, http://www.umin.ac.jp/ctrj/). The diagnosis of AML was on the basis of the French–American–British (FAB) classification.[26] Median follow-up time was 32.5 months. The age distribution is presented in Table 1. In the AML201 study, patients were randomly assigned to receive either IDR or HiDNR for induction therapy, and those who achieved CR were again randomized to receive either four courses of conventional consolidation therapy or three courses of HiDAC therapy.[24,25] Of the 197 patients, 98 and 99 patients were assigned to IDR and HiDNR arms for induction therapy, respectively. CR was achieved in 161 of 197 (81.7%) patients, and 80 and 77 patients were assigned to HiDAC and conventional consolidation therapies, respectively (Table 1).

High molecular weight DNA and total RNA were extracted from bone marrow samples using standard methods.[27–29]

Cytogenetic G-banding analysis was performed by standard methods. We also examined 11 chimeric gene transcripts (Major: *BCR-ABL1*, Minor: *BCR-ABL1*, *PML-RARA*, *RUNX1-RUNX1T1*, *CBFB-MYH11*, *DEK-NUP214*, *NUP98-HOXA9*, *MLL-MLLT1*, *MLL-MLLT2*, *MLL-MLLT3*and *MLL-MLLT4*) by reverse transcriptase-mediated quantitative PCR as previously reported.[30]

Morphological diagnosis, the FAB classification and karyotypes were reviewed and confirmed by the central review committees of the JALSG using the BM samples obtained at diagnosis.

We obtained informed consent from all patients to use their samples for banking and molecular analysis, and approval was obtained from the ethics committees of the participating institutes.

Screening for mutations in 51 genes

A custom-made oligonucleotide probe library was designed to capture the exons of 51 genes that have been recurrently identified in myeloid neoplasm (Supplementary Table 1). Captured and enriched exons were subjected to sequencing on an Illumina HiSeq (Illumina, San Diego, CA, USA).[31–33] Sequence variation annotation was performed using known polymorphism databases, followed by mutation characterization. Each predicted variant sequence was confirmed by Sanger sequencing. Internal tandem duplication of the *FLT3* gene (*FLT3*-ITD) and partial tandem duplication of the *MLL* gene (*MLL*-PTD) were examined as previously reported.[28,34]

Table 1. Characteristics of the 197 patients

Characteristics	*Number*	*(%)*
Age (year)		
15–19	6	3.0
20–29	32	16.2
30–39	35	17.8
40–49	33	16.8
50–59	69	35.0
60–64	22	11.2
FAB subtype		
M0	7	3.6
M1	36	18.3
M2	89	45.2
M4	34	17.3
M4Eo	9	4.6
M5	21	10.7
M6	1	0.51
Cytogenetic-risk group		
Favorable	55	27.9
RUNX1-RUNX1T1	41	20.8
CBFB-MYH11	14	7.1
Intermediate	100	50.8
Normal cytogenetics	72	36.5
Unfavorable	23	11.7
Complex karyotype	16	8.1
t(11q23) excluding t(9;11) and t(11;19)	3	1.5
t(9;22)	2	1.0
−7	1	0.5
Not determined	19	9.6
Induction therapy		
IDR + Ara-C	98	49.7
DNR + Ara-C	99	50.3
Achieving CR	161	81.7
Consolidation therapy		
High-dose Ara-C	80	51.0
Multiagent CT	77	49.0

Abbreviation: IDR, idarubicin. The study population included 197 newly diagnosed *de novo* AML patients except for acute promyelocytic leukemia, and equally assigned to induction and consolidation arms. Nine patients showed the M4Eo FAB type, and all of them harbored the *CBFB-MYH11* transcript.

Statistical analysis

Differences in continuous variables were analyzed by the unpaired *t*-test or the Mann–Whitney *U*-test for distribution between two groups. Analysis of frequencies was performed using Fisher's exact test for 2×2 tables or Pearson's χ^2 test for larger tables. A multivariate analysis to identify risk factors for achieving CR was performed by the logistic regression model. Survival probabilities were estimated by the Kaplan–Meier method, and differences in the survival distributions were evaluated using the log-rank test. OS was defined as the time from the date of entry into the AML201 study to death due to any cause or last follow-up. Disease-free survival (DFS) was defined as the time from the day of achieving CR to relapse, death due to any cause or last follow-up. Patients undergoing SCT were not censored at the time of transplantation. The prognostic significance of the clinical variables was assessed using the Cox proportional hazards model. These statistical analyses were performed with Prism 5 (GraphPad Software, La Jolla, CA, USA) and JMP Pro10 (SAS Institute Japan,

Tokyo, Japan). For all analyses, the *P*-values were two-tailed, and a *P*-value of less than 0.05 was considered statistically significant.

RESULTS

Cytogenetic analysis

Cytogenetic analysis revealed a normal karyotype in 72 (36.5%) patients and an abnormal karyotype in 106 (53.8%) patients, including 41 AML with t(8;21) (q22;q22); *RUNX1-RUNX1T1* and 14 AML with inv(16) (p13q22); *CBFB-MYH11*. However, karyotypes could not be determined in 19 (9.6%) patients because we could not obtain sufficient mitotic cells. On the basis of the G-banding karyotype and chimeric transcript analyses, patients were assigned to favorable- ($n=55$, 27.9%), intermediate- ($n=100$, 50.8%) and adverse-risk ($n=23$, 11.7%) groups according to the refined MRC criteria (Table 1).[4]

Frequencies of mutations

We identified mutations in 44 of 51 genes analyzed in the 197 AML patients. However, there were only five genes (*FLT3, NPM1, CEBPA, DNMT3A* and *KIT*) that were mutated in more than 10% of the patients (Figure 1a and Supplementary Table 1). Each position and type of mutation is presented in Supplementary Figure 1. As germ-line controls were available in a limited number of patients, we could not completely confirm that all identified mutations were somatic mutations. Therefore, there is a possibility that a part of identified mutations might be rare SNPs. *FLT3* mutation was the most frequently identified (50 patients, 25.4%), followed by *NPM1* (38 patients, 19.2%), *DNMT3A* (32 patients, 16.2%), *CEBPA* (31 patients, 15.7%) and *KIT* mutations (28 patients, 14.2%). Of the 50 patients with *FLT3* mutations, 36 (18.3%) and 17 (8.6%) patients harbored *FLT3*-ITD and *FLT3*-KDM, respectively, and three patients harbored both mutations. Of the 31 patients with *CEBPA* mutations, 19 (9.6%) and 12 (6.1%) patients harbored double *CEBPA* (*CEBPA*-D) mutations and a single *CEBPA* (*CEBPA*-S) mutation, respectively. Of the 28 patients with *KIT* mutations, 4, 2 and 23 patients harbored mutations in exon 8, exons 10–11 and exon 17 of the *KIT* gene, respectively, and one patient harbored mutations in both exons 10–11 and exon 17.

Although mutations in the 51 analyzed genes were not identified in 14 (7.1%) patients, 183 (92.9%) patients harbored one or more mutations; one mutation in 36, two mutations in 56, three mutations in 40, four mutations in 27, five mutations in 17, six mutations in five and seven mutations in two patients. The mean mutation number per patient was 2.56 ± 0.11 in all patients, whereas it was significantly higher in patients with a normal karyotype (3.18 ± 0.16) than in those with an aberrant karyotype (2.10 ± 0.15) ($P<0.0001$). Furthermore, mean mutation numbers per patient in AML with *RUNX1-RUNX1T1* (1.68 ± 0.17) and *CBFB-MYH11* (1.57 ± 0.20) were significantly lower than that in all samples ($P=0.0008$ and 0.0123, respectively) (Figure 1b).

The mean mutation number per patient aged 60–64 years (3.18 ± 0.41) tended to be higher, although there was no significant difference between the mean mutation number and age (Supplementary Figure 2).

Genetic alterations found in AML have been conceptually grouped into class I mutation, which causes constitutive activation of intracellular signals that contribute to the growth and survival, and class II mutation that blocks differentiation and/or enhance self-renewal by altered transcription factors.[35–37] Recently, it has been suggested that mutations that modify the epigenetic status generate a new class because of their overlap mutations both with class I and class II mutations.[13,38] In this study, Class II mutations (*NPM1, CEBPA, RUNX1* and *GATA2* mutations, and *RUNX1-RUNX1T1* and *CBFB-MYH11*) were the most frequently identified (138/197; 70.1%), followed by Class I mutations (*FLT3, KIT, N/KRAS, PTPN11, JAK1/3* and *TP53* mutations) (116/197; 58.9%) and mutations that modify the epigenetic status (*ASXL1, ATRX, EZH2, TET2, PBRM1, DNMT3A, IDH1/2, KDM6A, MLL* and *DOT1L* mutations) (91/197; 46.2%). Furthermore, mutations of NOTCH family genes (*NOTCH1 and NOTCH2*), cohesin complex genes (*STAG2, SMC1A, SMC3* and *RAD21*), BCOR family genes (*BCOR* and *BCORL1*), NCOR family genes (*NCOR1, NCOR2* and *DIS3*) and spliceosome genes (*SF3B1, U2AF1, SRSF2* and *ZRSR2*) were identified in 19 (9.6%), 22 (11.2%), 17 (8.6%), 22 (11.2%) and 9 patients (4.6%), respectively (Figure 1c).

Association between gene mutations and cytogenetics

The prevalence of each gene mutation differed among the cytogenetic-risk groups. *KIT* mutations were preferentially identified in the favorable cytogenetic-risk group. *FLT3*-ITD, *NPM1, CEBPA* and *DNMT3A* mutations were preferentially identified in the intermediate-risk group, particularly in patients with a normal karyotype. *BCORL1* and *TP53* mutations were preferentially identified in the poor-risk group; in particular, *TP53* mutations were frequent in patients with a complex karyotype. In addition, *PHF6* mutations were also frequently identified in patients with a complex karyotype (Figure 2 and Supplementary Table 2).

Overlap mutations

Several patterns of overlap mutations were identified in this comprehensive mutation analysis (Supplementary Figures 3 and 4). Significantly overlapped mutations were observed between *FLT3* mutations and *NPM1, DNMT3A* and *MLL*-PTD mutations; *NPM1* mutations and *DNMT3A, IDH1* and *IDH2* mutations; *CEBPA* mutations and *TET2* mutations; *ASXL1* mutations and spliceosome gene mutations; *DIS3* mutations and *MLL* mutations; *DNMT3A* mutations and *PTPN11* mutations; *GATA2* mutations and *CEBPA*-D mutations; *K/NRAS* mutations and *WT1* mutations and *BCOR/BCORL1* mutations; *RUNX1* mutations and *U2AF1, MLL-PTD, BCOR/BCORL1* and *PHF6* mutations; *SF3B1* mutations and *NRAS* mutations; and *TET2* mutations and *STAG2* mutations. In contrast, mutually exclusive mutations were observed between *FLT3* mutations and *KIT, K/NRAS* and *CEBPA*-D mutations; *NPM1* mutations and *CEBPA*-D and *RUNX1* mutations; and *CEBPA* mutations and *IDH1/2* mutations.

According to the conceptual classification of the mutated genes, overlap mutations between Class I, Class II and epigenetic modifying gene mutations were frequently observed. However, these major mutations widely coexisted with other family gene mutations, such as the cohesin complex, BCOR family and spliceosome gene mutations (Figure 1d). Although biological functions of mutated genes have not been fully clarified, we also present frequencies and associations of mutated genes according to the provisional gene function in the Supplementary Figure 5.

Association of gene mutations with clinical characteristics

Several associations between mutations and clinical characteristics were observed. *DNMT3A* mutations and *MLL*-PTD were more frequently identified in patients over 50 years old than in those less than 50 years old ($P=0.0064$ and $P=0.0121$, respectively), whereas the other mutations were not significantly associated with age (Supplementary Table 3).

Several mutations were associated with the white blood cell count at diagnosis. *FLT3-ITD, NPM1, DNMT3A* and *NOTCH1* mutations were significantly associated with the high white blood cell count. In contrast, *ASXL1* and *IDH1* mutations were associated with a lower white blood cell count (Supplementary Table 4).

Association of gene mutations with the CR rate

We analyzed the association of mutations with the CR rate. By Fisher's exact test, *RUNX1-RUNX1T1* or *CBFB-MYH11, KIT, NPM1* and *CEBPA*-D mutations were identified as favorable factors for

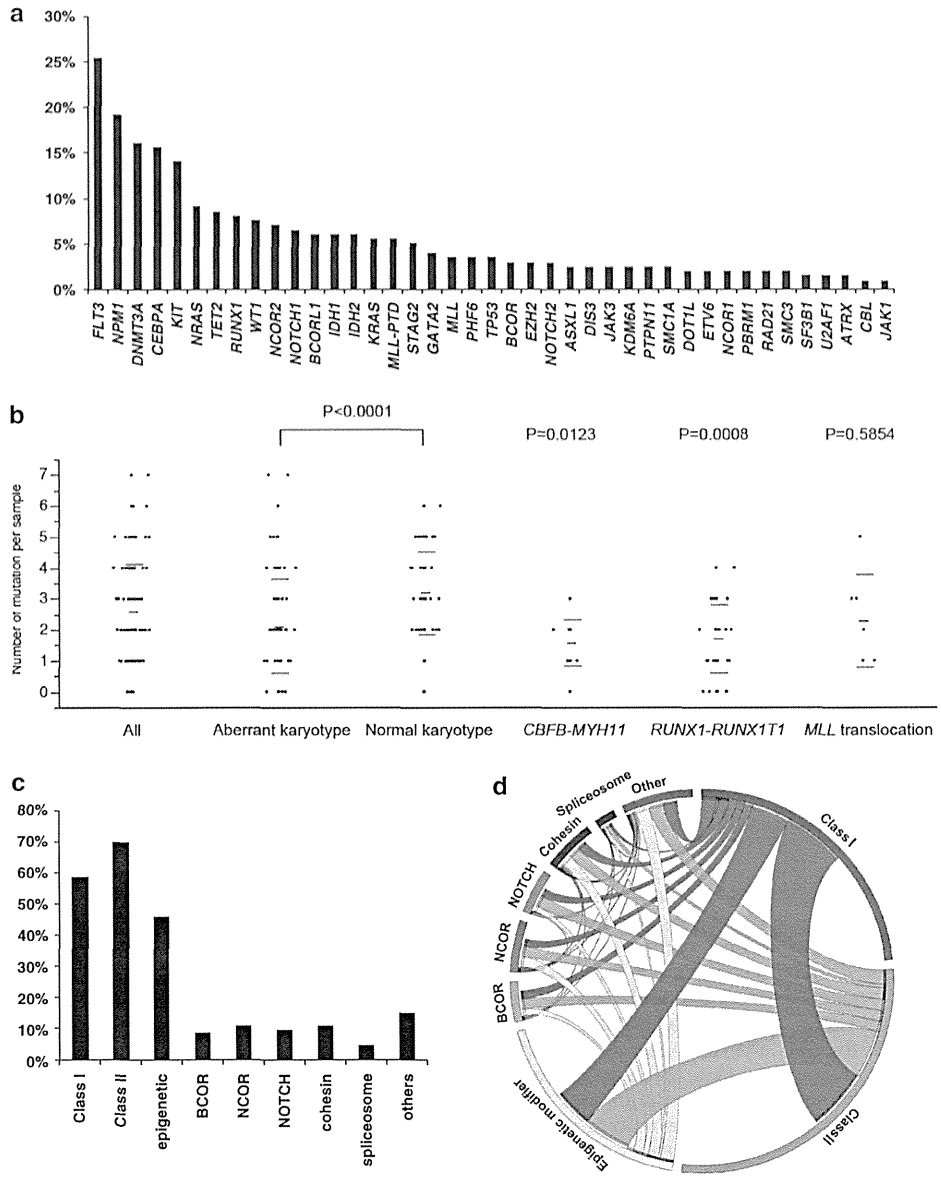

Figure 1. Frequencies and associations of mutated genes. (**a**) Frequencies of analyzed gene mutations. Frequency of each mutated gene is shown. Mutations were identified in 44 genes of 51 genes analyzed in 197 AML patients. Only five genes (*FLT3, NPM1, CEBPA, DNMT3A* and *KIT*) were mutated in more than 10% of the patients. (**b**) Mutated gene numbers according to the cytogenetics. Mean mutation number ± s.d. is indicated by horizontal lines. Mean mutation number per one patient in patients with normal karyotype (3.18 ± 0.16) was significantly higher than in that with aberrant karyotype (2.10 ± 0.15) ($P<0.0001$). Those in AML with *RUNX1-RUNX1T1* (1.68 ± 0.17) and *CBFB-MYH11* (1.57 ± 0.20) were significantly lower than that in all samples ($P=0.0008$ and $P=0.0123$, respectively). That in AML with *MLL*-translocation tended to be lower but not statistically significant (2.28 ± 0.57, $P=0.5854$). (**c**) Frequencies of mutations according to the conceptual classification. Mutations in Class I, Class II and epigenetic modifying genes were frequently identified. (**d**) Association of mutated genes according to the conceptual classification. Circos plot of mutated genes according to the function is shown.[45] Overlap mutations between Class I, Class II and epigenetic modifying genes mutations were frequently observed. These major mutations were widely coexistent with another family genes, such as cohesin complex, BCOR family and spliceosome genes.

achieving CR, and *TP53* mutation was an unfavorable factor; however, multivariate logistic regression analysis including all analyzed mutations showed that only *NPM1* (Hazard ratio (HR): 96.206, 95% Confidence interval (CI): 2.247–411.9, $P=0.0172$) and *TP53* (HR: 22.222, 95% CI: 1.597–333.3, $P=0.0172$) mutations were identified as favorable and unfavorable factors for achieving CR, respectively (Table 2 and Supplementary Table 5).

Importantly, *KIT* mutations were closely associated with *RUNX1-RUNX1T1* or *CBFB-MYH11*, whereas the other mutations that confer the achievement of CR were mutually exclusive (Supplementary Figures 3 and 6). In the patients with *RUNX1-RUNX1T1* or *CBFB-MYH11, NPM1* and *CEBPA*-D mutations, the CR rate (106/112; 94.6%) was significantly higher than for those with the other genotypes (55/85; 64.7%) ($P<0.0001$).

Prognostic impacts of mutations

We next analyzed the prognostic impact of each mutation. By univariate analysis, *FLT3*-ITD (HR: 1.805, 95% CI: 1.130–2.885, $P=0.0135$), *DNMT3A* (HR: 1.696, 95% CI: 1.055–2.725, $P=0.0291$),

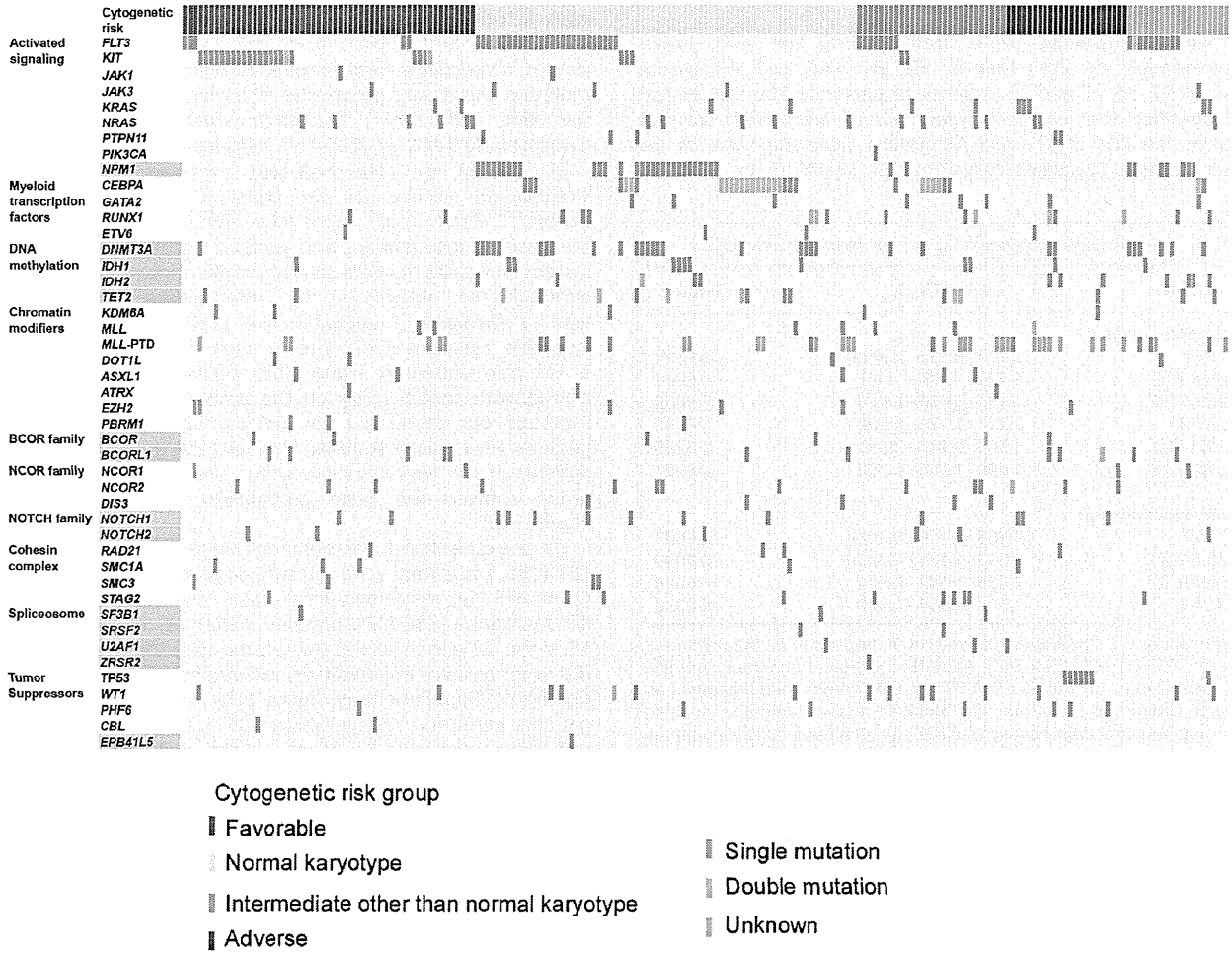

Figure 2. Mutation status according to the cytogetics-risk groups. Identified mutations in analyzed AML patients are shown according to the cytogenetic-risk groups. Pink boxes indicate single mutations and orange boxes indicate double mutations.

Table 2. Gene mutations affecting the CR achievement

Mutations	*CR rate (%)*		P-*value*
	Positive	*Negative*	
Fisher's exact test			
NPM1	97	78	0.0041
CEBPA-D-Mt.	100	80	0.0273
KIT	96	79	0.0326
RUNX1-RUNX1T1 or *CBFB-MYH11*	91	78	0.0409
TP53	14	84	0.0002

Mutations	*HR (95% CI)*	P-*value*
Multivariate analysis		
Wild-*NPM1*	96.206 (2.247–411.9)	<0.0001
TP53 mutation	22.222 (1.597–333.3)	0.0172

Abbreviations: CI, confidence interval; CR, complete remission; HR, hazard ratio. By the Fisher's exact test, *RUNX1-RUNX1T1* or *CBFB-MYH11*, *KIT*, *NPM1* and *CEBPA*-D mutations were identified as the favorable factor for achieving CR, and *TP53* mutation was for the unfavorable factor. The multivariate logistic regression analysis including all analyzed mutations showed that only wild-*NPM1* and *TP53* mutation were identified as unfavorable factors for achieving CR.

TP53 (HR: 15.167, 95% CI: 6.555–35.094, $P<0.001$), *MLL*-PTD (HR: 3.782, 95% CI: 1.948–7.346, $P<0.001$) and *RUNX1* (HR: 2.301, 95% CI: 1.278–4.146, $P=0.0055$) mutations and the karyotypes other than *RUNX1-RUNX1T1* or *CBFB-MYH11* (HR: 2.786, 95% CI: 1.608–4.831, $P=0.0003$) were identified as unfavorable prognostic factors for OS (Table 3 and Supplementary Figure 7). Multivariate Cox regression analysis with stepwise selection showed that *TP53* (HR: 14.803, 95% CI: 6.259–35.009, $P<0.001$), *MLL*-PTD (HR: 2.853, 95% CI: 1.401–5.810, $P=0.0039$) and *RUNX1* (HR: 1.965, 95% CI: 1.054–3.663, $P=0.0336$) mutations and the karyotypes other than *RUNX1-RUNX1T1* or *CBFB-MYH11* (HR: 2.353, 95% CI: 1.342–4.132, $P=0.0028$) were independent poor prognostic factors for OS (Table 3).

In this cohort, mutations of NOTCH family, the cohesin complex, BCOR family and spliceosome genes were frequently identified. NOTCH family and BCOR family genes were not associated with the CR rate, OS and DFS. Although mutations of cohesin complex genes were not associated with the CR rate and DFS, the patients harboring those mutations revealed better OS than those without mutations ($P=0.0274$) (Figure 3). The CR rate and DFS of patients with spliceosome gene mutations tended to be lower than for those without mutations, although both differences were not statistically significant: the CR was achieved in five of the nine (55.6%) and 156 of the 188 (83.0%) patients ($P=0.0601$), and 3-year DFS were 0% and 38.9% ($P=0.1117$) in those with and

without mutations, respectively (Supplementary Table 3 and Supplementary Figure 8).

When the patients were stratified into the risk groups recommended by ELN, that is, FR, IR-I, IR-II and AR groups included 92, 35, 42 and 28 patients, respectively. The ELN system well stratified the long-term prognosis of adult AML patients, whereas the OSs of IR-I and AR groups were the same in the present cohort (Supplementary Figure 9). Therefore, we analyzed whether another mutations could further stratify the prognosis in each ELN-risk group. *MLL*-PTD, *GATA2* and *TP53* mutations were identified as further poor prognostic factors in IR-I, IR-II and AR groups, respectively. Furthermore, we identified that the *DNMT3A* mutation was a poor prognostic factor in the FR group except for the AML with t(8;21) (q22;q22); *RUNX1-RUNX1T1* or inv(16) (p13q22); *CBFB-MYH11* (CBF-AML) (Figure 4).

Table 3. Unfavorable prognostic factors for overall survival (OS)

Mutations	*HR (95% CI)*	P-*value*
Univariate analysis		
TP53	15.167 (6.555–35.094)	<0.0001
MLL-PTD	3.782 (1948–7.346)	<0.0001
Non CBF	2.786 (1.608–4.831)	0.0003
RUNX1	2.301 (1.278–4.146)	0.0055
FLT3-ITD	1.805 (2.247–4119)	0.0135
DNMT3A	1.696 (1.055–2.725)	0.0291
Multivariate analysis		
TP53	14.803 (6.259–35.009)	<0.0001
MLL-PTD	2.853 (1.4017–5.810)	0.0039
Non CBF	2.353 (1.342–4.132)	0.0028
RUNX1	1.965 (1.054–3.663)	0.0336

Abbreviations: CI, confidence interval; HR, hazard ratio. By the univariate analysis, *FLT3*-ITD, *DNMT3A*, *TP53*, *MLL*-PTD and *RUNX1* mutations and the karyotypes other than *RUNX1-RUNX1T1* or *CBFB-MYH11* were identified as adverse prognostic factors for OS. Multivariate Cox regression analysis with stepwise selection showed that *TP53*, *MLL*-PTD and *RUNX1* mutations and the karyotypes other than *RUNX1-RUNX1T1* or *CBFB-MYH11* were independent poor prognostic factors for OS.

In addition, we also evaluated two recently reported risk stratification systems on the basis of genetic status in our cohort.[5,39] Patel *et al.*[5] reported a risk stratification system on the basis of cytogenetics and genetic status According to their system, our patients were clearly stratified into three risk groups, although the patients in the intermediate cytogenetic risk with a favorable mutational risk profile and those in the favorable cytogenetic-risk profile showed the same probability of OS (Supplementary Figure 10a). Grossmann *et al.*[39] reported a prognostic model solely on the basis of molecular mutations. Although our cohort did not include AML with *PML-RARA*, our patients were clearly stratified into four risk groups. However, the patients in the very favorable group and those in the favorable group showed the same probability of OS (Supplementary Figure 10b).

On the other hand, *KIT* mutations were frequently identified in CBF-AML, while they were not a poor prognostic factor for either OS or DFS (Supplementary Figure 11a). According to the types of *KIT* mutations, CBF-AML patients harboring mutations in exon 17 of the *KIT* gene showed worse prognosis than those harboring the other types of *KIT* mutation, although this was not statistically significant (Supplementary Figure 11b). Notably, in the CBF-AML patients harboring *KIT* mutations, OS and DFS of those treated with three courses of HiDAC consolidation therapy tended to be better than those treated with four courses of conventional standard-dose multiagent therapy (Supplementary Figure 11c).

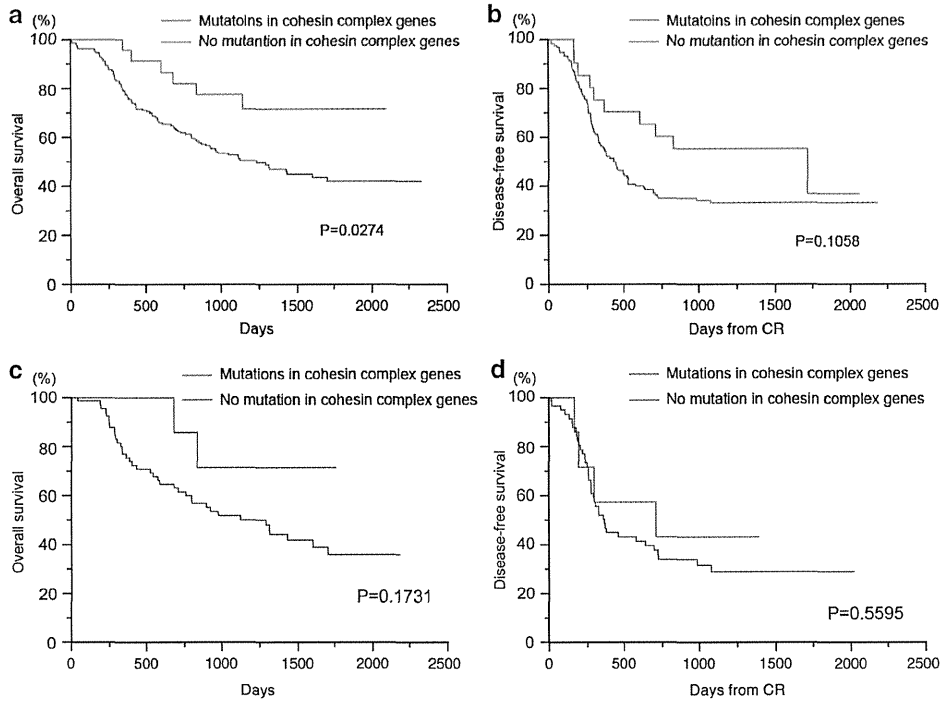

Figure 3. Prognostic impact of mutations in cohesin complex genes. Kaplan–Meier curves for OS and DFS according to the mutations in cohesin complex genes are shown. (**a**) OS in the total patients, (**b**) DFS in the total patient, (**c**) OS in the patients with normal karyotype, (**d**) DFS in the patients with normal karyotype. Although mutations of cohesin complex genes were not associated with the CR rate and DFS, the patients harboring those mutations revealed better OS than those without mutations ($P = 0.0274$). In the patients with normal karyotype, OS of the mutated patients tended to be better that that of unmutated patients, though statistical significance was not observed ($P = 0.1731$).

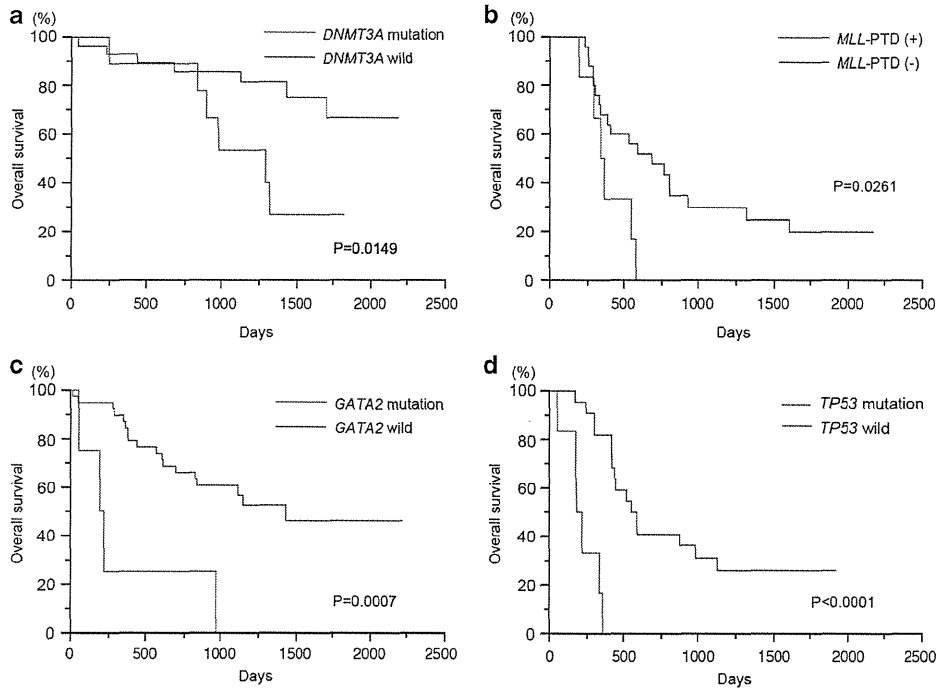

Figure 4. Mutations that could further stratify the ELN-risk groups into two risk groups. (**a**) *DNMT3A* mutation was a poor prognostic factor in the FR group except for the AML with t(8;21) (q22;q22); *RUNX1-RUNX1T1* or inv(16) (p13q22); *CBFB-MYH11* (CBF-AML). (**b**) *MLL*-PTD was a poor prognostic factor for the OS in the ELN IR-I group. (**c**) *GATA2* mutation was a poor prognostic factor for the OS in the ELN IR-II group. (**d**) *TP53* mutation was a poor prognostic factor for the OS in the ELN AR group.

In CBF-AML, the accumulated mutation number was lower than in the other types of AML, although many kinds of mutation were identified (Supplementary Figure 12). However, we could not identify a gene that affects the prognosis of CBF-AML.

Taking these results together, we tried to modify the genetic criteria for the ELN stratification system. When the CN-AML patients with *DNMT3A* mutations of the FR group and the patients with *MLL*-PTD of the IR-I group were included in the IR-I and the AR group, respectively, we could more clearly stratified the patients into four risk groups for OS than the original ELN system (Figures 5a and b). Furthermore, as the prognosis of the patients with *TP53* mutations were very unfavorable as previously reported,[39] we could more clearly stratify the patients into five risk groups for OS by classifying the *TP53*-mutated patients as the very adverse-risk group (Figures 5c and d).

DISCUSSION

In this study, we comprehensively analyzed mutations of 51 genes by the targeting sequence, and identified a total of 505 mutations in 44 genes in 197 adult *de novo* AML patients except for APL. The whole-genome and -exome analysis demonstrated recurrent mutations in a total of 260 genes in 200 AML patients, suggesting that another mutations might be accumulated in the presently analyzed AML cells.[40] However, frequencies of most mutated genes were reportedly less than 10%. In consistence, only five genes (*FLT3, NPM1, CEBPA, DNMT3A* and *KIT*) were mutated in more than 10% patients in our study, and each mutation frequency was almost the same as previous reports.[5,17,19,39] The frequency of *KIT* mutation was relatively higher in our study than previous reports,[5,40] while this is caused by the higher frequency of CBF-AML (28.0%) in the Japanese patients, in which *KIT* mutations are frequently identified. Our study, therefore, essentially includes major genetic regions, which may affect the pathogenesis and prognosis of AML. However, mutation analyses were not thoroughly performed in all subtypes of AML, such as acute erythroid leukemia and acute megakaryoblastic leukemia because of their lower frequencies. Further analyses are required to fully clarify the genetic alterations in AML.

The whole-genome and -exome analysis demonstrated that an average of mutated genes in coding regions per sample was 5.24.[40] Of note was that there were significant differences in mutated gene numbers among the types of cytogenetics and mutations: the mean mutation numbers were higher in AML with *RUNX1-RUX1T1*, and are lower in that with *PML-RARA* and *MLL* translocations than that of all samples. As analyzed gene numbers were limited, mean mutated gene number per sample (2.56 ± 0.11) was low in our study; however, there were different features from the previous report. In our study, higher mutation number was observed in CN-AML (3.18 ± 0.16), and lower was in CBF-AML. Furthermore, the mutation number in AML with *MLL*-translocation tended to be lower (2.28 ± 0.57, $P = 0.5854$). These results collectively suggested that recurrent cytogenetic abnormalities, such as *RUNX1-RUNX1T1, CBFB-MYH11* and *MLL*-translocation, have a strong potential for the initiation of AML, and that most of accumulated mutations in AML with these cytogenetics might be passenger mutations.

It has been reported that common mutations in AML, such as *DNMT3A, NPM1, CEBPA, IDH1/2* and *RUNX1*, were mutually exclusive of the transcription-factor fusions, indicating the high potential for leukemia initiation.[10,11,13,40,41] Consistently, *DNMT3A, NPM1* and *CEBPA* mutations were not identified in CBF-AML, but frequent in CN-AML. In addition, we identified that *MLL*-PTD mutation was also exclusive of CBF-AML. In CBF-AML, *KIT* mutations were preferentially identified, whereas several types of mutations were also accumulated, suggesting that many mutations could act as a driver mutation for the clonal expansion of the initiating clone with *RUNX1-RUNX1T1* and

a

Genetic group	Subsets
Favorable	• CBF-AMLs • CN-AMLs with mutated *NPM1* without *FLT3*-ITD and mutated *DNMT3A* (normal karyotype) • CN-AMLs with mutated *CEBPA* without mutated *DNMT3A* (normal karyotype)
Intermediate-I	• CN-AMLs with mutated *DNMT3A* • CN-AMLs except for those included in the FR and AR
Intermediate-II	• AMLs included in the IR-II of the ELN stratification
Adverse	• CN-AMLs with *MLL*-PTD • AMLs included in the AR of the ELN stratification

b

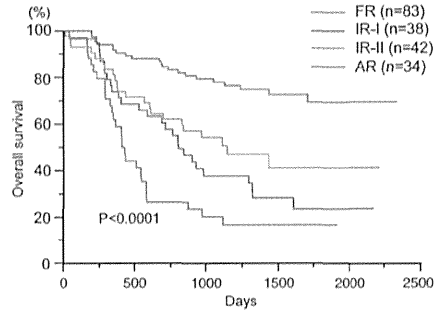

c

Genetic group	Subsets
Favorable	• CBF-AMLs • CN-AMLs with mutated *NPM1* without *FLT3*-ITD and mutated *DNMT3A* (normal karyotype) • CN-AMLs with mutated *CEBPA* without mutated *DNMT3A* (normal karyotype)
Intermediate-I	• CN-AMLs with mutated *DNMT3A* • CN-AMLs except for those included in the FR and AR
Intermediate-II	• AMLs included in the IR-II of the ELN stratification except for those with mutated *TP53*
Adverse	• CN-AMLs with *MLL*-PTD • AMLs included in the AR of the ELN stratification except for those with mutated *TP53*
Very Adverse	• AMLs with mutated *TP53*

d

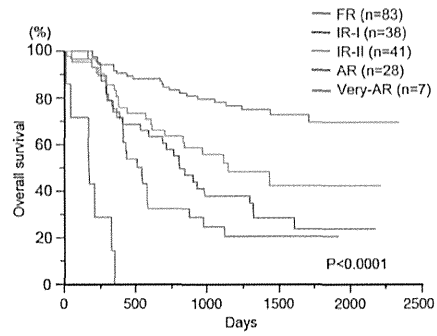

Figure 5. Risk stratification by modifying the ELN stratification system. When the CN-AML patients with *DNMT3A* mutations of the FR group and the patients with *MLL*-PTD of the IR-I group were included in the IR-I and the AR group, respectively (**a**), we could more clearly stratify the patients into four risk groups for OS than the original ELN system (**b**). When the patients with *TP53* mutations were classified as the very adverse-risk group (**c**), we could more clearly stratify the patients into five risk groups for OS (**d**).

CBFB-MYH11. Further study is required to clarify which combination is necessary for the clonal expansion, and whether different combinations cause clinical and phenotypical varieties.

After the completion of genetic alterations in AML, the most important issue is to clarify the prognostic impact of each mutation and/or co-occurring mutations.[7,42] The recently recommended ELN classification system is the first system that includes both cytogenetics and mutation status. Several groups reported that the ELN system clearly stratified the long-term prognosis of AML patients. However, the prognosis of FR groups except for the CBF-AML is still controversial. Paschka *et al.*[43] reported that the *IDH1/2* mutation was a poor prognostic factor in CN-AML with mutated *NPM1* without *FLT3*-ITD. In contrast, Patel *et al.*[5] reported that the *IDH1/2* mutation was a favorable prognostic factor in AML with mutated *NPM1* without *FLT3*-ITD. Furthermore, it has been reported that the *TET2* mutation was an adverse prognostic factor in AML with mutated *NPM1* or *CEBPA* without *FLT3*-ITD.[22] In the present cohort, we could not observe the statistically significant effects of *IDH1/2* and *TET2* mutations on the prognosis of CN-AML with mutated *NPM1* or *CEBPA* without *FLT3*-ITD, while we identified that *DNMT3A* mutation is an adverse prognostic factor in CN-AML with mutated *NPM1* or *CEBPA* without *FLT3*-ITD. In addition, we could not find the better prognostic impact of the *CEBPA* double mutations on the FR group recommended by the ELN in contrast to previous reports.[39,44]

Although different mutations might further stratify the prognosis of AML with mutated *NPM1* or *CEBPA* without *FLT3*-ITD, it was noteworthy that all mutations belonged to the class modifying methylation status.[13,38] These results collectively suggested that the epigenetic deregulation might contribute the pathogenesis of AML with mutated *NPM1* or *CEBPA* without *FLT3*-ITD. Prospective and large-scale study is necessary to clarify what genetic alterations influence the prognosis of AML with these genotypes.

In this study, we demonstrated that the prognosis of adult AML patients could be more clearly stratified by including the *DNMT3A* and *MLL*-PTD mutation status than the original ELN system, and that *TP53* mutations have a very adverse effect on the prognosis of AML patients. However, as most recurrently identified mutations were observed less than 5% of AML, it is highly expected to refine the genetic-based risk stratification system by much larger-scale studies. In addition, it is also important to evaluate the prognostic effects according to the functions of mutated genes rather than each sole mutation.

In the JALSG AML201 study, patients were randomized to the standard dose of IDR + Ara-C or HiDNR + Ara-C induction therapy, and the CR patients were again randomized to three courses of HiDAC or four courses of conventional standard-dose multiagent consolidation therapy. Therefore, we analyzed whether therapeutic regimens affect the CR rate and long-term survivals according to the mutation status and risk groups on the basis of the genetic status, while we could not observe any significant differences between therapeutic regimens and genetic status. Furthermore, we could not demonstrate that allo-SCT could improve the prognosis of the patients falling in the intermediate- and adverse-risk groups because of the small number of patients who underwent allo-SCT in the first CR in this cohort. It is, therefore, required to evaluate whether therapeutic regimens and allo-SCT affect the prognosis according to the genetic status.

In conclusion, we comprehensively analyzed 51 genes mutations in 197 *de novo* adult AML patients who were registered to a single prospective clinical study, and demonstrated that cooperative and exclusive mutation patterns and their prognostic impacts. Furthermore, we demonstrated that the prognosis of adult AML patients could be more clearly stratified by including the *DNMT3A*, *MLL*-PTD and *TP53* mutation status than the original ELN system. However, prognostic impacts of some mutation status are different from the previous reports. We must refine the risk

stratification system by considering all known-risk factors in a large-scale and well-established cohort, although molecular genetic status has a strong impact on the prognosis of AML patients. We are now conducting a prospective large-scale study to confirm the present results.

CONFLICT OF INTEREST

H Kiyoi: Research funding from Bristol-Myers Squibb, Novartis Pharma, Chugai Pharmaceutical Co., Ltd. and Kyowa Hakko Kirin Co., Ltd. YM: Honoraria from Bristol-Myers Squibb, Novartis Pharma, Chugai Pharmaceutical Co., Ltd., Kyowa Hakko Kirin Co., Ltd. and Celgene Japan; Research funding from Bristol-Myers Squibb, Novartis Pharma, Chugai Pharmaceutical Co., Ltd. and Kyowa Hakko Kirin Co., Ltd. NU: Consultant for Kyowa Hakko Kirin Co., Ltd.; Honoraria from Bristol-Myers Squibb, Novartis Pharma and Chugai Pharmaceutical Co., Ltd.; Research funding from Bristol-Myers Squibb, Novartis Pharma, Chugai Pharmaceutical Co., Ltd. and Kyowa Hakko Kirin Co., Ltd. TN: Research funding from Bristol-Myers Squibb, Novartis Pharma, Chugai Pharmaceutical Co., Ltd., Kyowa Hakko Kirin Co., Ltd., Dainippon Sumitomo Pharma and Zenyaku Kogyo. The other authors declare no conflict of interest.

ACKNOWLEDGEMENTS

This study was performed as a research program of the Project for Development of Innovative Research on Cancer Therapeutics (P-Direct), Ministry of Education, Culture, Sports, Science and Technology of Japan, and was also supported by Grants-in-Aid from the Scientific Research Program from the Japanese Ministry of Education, Culture, Sports, Science, and Technology, the Ministry of Health, Labor and Welfare for Cancer Research (Clinical Cancer Research H23-004 and H25-006), the National Cancer Center Research and Development Fund (23-A-23) and from KAKENHI (22134006 and 23249052).

AUTHOR CONTRIBUTIONS

H Kiyoi, S Ogawa and TN designed the study, interpreted the data and wrote the manuscript; RK, YN, T Kato, EY, KS and FC performed molecular analysis and interpreted the data; YN, YS, KC, HT, SM and S Ogawa performed bioinformatics; NA, S Ohtake, SM, YM, TS, YO, N Usui, H Kanamori, T Kiguchi, KI, N Uike, FK, KK, CN, MO, AT, FI, HS, YK and HM collected samples and clinical data, contributed to the interpretation of the data and critically reviewed the draft; and all authors approved the final version submitted for the publication.

REFERENCES

1 Estey E, Dohner H. Acute myeloid leukaemia. *Lancet* 2006; **368**: 1894–1907.
2 Dohner H, Estey EH, Amadori S, Appelbaum FR, Buchner T, Burnett AK *et al.* Diagnosis and management of acute myeloid leukemia in adults: recommendations from an international expert panel, on behalf of the European LeukemiaNet. *Blood* 2010; **115**: 453–474.
3 Koreth J, Schlenk R, Kopecky KJ, Honda S, Sierra J, Djulbegovic BJ *et al.* Allogeneic stem cell transplantation for acute myeloid leukemia in first complete remission: systematic review and meta-analysis of prospective clinical trials. *JAMA* 2009; **301**: 2349–2361.
4 Grimwade D, Hills RK, Moorman AV, Walker H, Chatters S, Goldstone AH *et al.* Refinement of cytogenetic classification in acute myeloid leukemia: determination of prognostic significance of rare recurring chromosomal abnormalities among 5876 younger adult patients treated in the United Kingdom Medical Research Council trials. *Blood* 2010; **116**: 354–365.
5 Patel JP, Gonen M, Figueroa ME, Fernandez H, Sun Z, Racevskis J *et al.* Prognostic relevance of integrated genetic profiling in acute myeloid leukemia. *N Engl J Med* 2012; **366**: 1079–1089.
6 Shen Y, Zhu YM, Fan X, Shi JY, Wang QR, Yan XJ *et al.* Gene mutation patterns and their prognostic impact in a cohort of 1185 patients with acute myeloid leukemia. *Blood* 2011; **118**: 5593–5603.
7 Ofran Y, Rowe JM. Genetic profiling in acute myeloid leukaemia—where are we and what is its role in patient management. *Br J Haematol* 2013; **160**: 303–320.
8 Delhommeau F, Dupont S, Della Valle V, James C, Trannoy S, Masse A *et al.* Mutation in TET2 in myeloid cancers. *N Engl J Med* 2009; **360**: 2289–2301.
9 Langemeijer SM, Kuiper RP, Berends M, Knops R, Aslanyan MG, Massop M *et al.* Acquired mutations in TET2 are common in myelodysplastic syndromes. *Nat Genet* 2009; **41**: 838–842.
10 Mardis ER, Ding L, Dooling DJ, Larson DE, McLellan MD, Chen K *et al.* Recurring mutations found by sequencing an acute myeloid leukemia genome. *N Engl J Med* 2009; **361**: 1058–1066.
11 Ley TJ, Ding L, Walter MJ, McLellan MD, Lamprecht T, Larson DE *et al.* DNMT3A mutations in acute myeloid leukemia. *N Engl J Med* 2010; **363**: 2424–2433.
12 Nikoloski G, Langemeijer SM, Kuiper RP, Knops R, Massop M, Tonnissen ER *et al.* Somatic mutations of the histone methyltransferase gene EZH2 in myelodysplastic syndromes. *Nat Genet* 2010; **42**: 665–667.
13 Shih AH, Abdel-Wahab O, Patel JP, Levine RL. The role of mutations in epigenetic regulators in myeloid malignancies. *Nat Rev Cancer* 2012; **12**: 599–612.
14 Chou WC, Huang HH, Hou HA, Chen CY, Tang JL, Yao M *et al.* Distinct clinical and biological features of *de novo* acute myeloid leukemia with additional sex comb-like 1 (ASXL1) mutations. *Blood* 2010; **116**: 4086–4094.
15 Grossmann V, Tiacci E, Holmes AB, Kohlmann A, Martelli MP, Kern W *et al.* Whole-exome sequencing identifies somatic mutations of BCOR in acute myeloid leukemia with normal karyotype. *Blood* 2011; **118**: 6153–6163.
16 Li M, Collins R, Jiao Y, Ouillette P, Bixby D, Erba H *et al.* Somatic mutations in the transcriptional corepressor gene BCORL1 in adult acute myelogenous leukemia. *Blood* 2011; **118**: 5914–5917.
17 Welch JS, Ley TJ, Link DC, Miller CA, Larson DE, Koboldt DC *et al.* The origin and evolution of mutations in acute myeloid leukemia. *Cell* 2012; **150**: 264–278.
18 Yoshida K, Sanada M, Shiraishi Y, Nowak D, Nagata Y, Yamamoto R *et al.* Frequent pathway mutations of splicing machinery in myelodysplasia. *Nature* 2011; **478**: 64–69.
19 Naoe T, Kiyoi H. Gene mutations of acute myeloid leukemia in the genome era. *Int J Hematol* 2013; **97**: 165–174.
20 Rollig C, Bornhauser M, Thiede C, Taube F, Kramer M, Mohr B *et al.* Long-term prognosis of acute myeloid leukemia according to the new genetic risk classification of the European LeukemiaNet recommendations: evaluation of the proposed reporting system. *J Clin Oncol* 2011; **29**: 2758–2765.
21 Mrozek K, Marcucci G, Nicolet D, Maharry KS, Becker H, Whitman SP *et al.* Prognostic significance of the European LeukemiaNet standardized system for reporting cytogenetic and molecular alterations in adults with acute myeloid leukemia. *J Clin Oncol* 2012; **30**: 4515–4523.
22 Metzeler KH, Maharry K, Radmacher MD, Mrozek K, Margeson D, Becker H *et al.* TET2 mutations improve the new European LeukemiaNet risk classification of acute myeloid leukemia: a Cancer and Leukemia Group B study. *J Clin Oncol* 2011; **29**: 1373–1381.
23 Miyawaki S. Clinical studies of acute myeloid leukemia in the Japan Adult Leukemia Study Group. *Int J Hematol* 2012; **96**: 171–177.
24 Ohtake S, Miyawaki S, Fujita H, Kiyoi H, Shinagawa K, Usui N *et al.* Randomized study of induction therapy comparing standard-dose idarubicin with high-dose daunorubicin in adult patients with previously untreated acute myeloid leukemia: the JALSG AML201 Study. *Blood* 2011; **117**: 2358–2365.
25 Miyawaki S, Ohtake S, Fujisawa S, Kiyoi H, Shinagawa K, Usui N *et al.* A randomized comparison of 4 courses of standard-dose multiagent chemotherapy versus 3 courses of high-dose cytarabine alone in postremission therapy for acute myeloid leukemia in adults: the JALSG AML201 Study. *Blood* 2011; **117**: 2366–2372.
26 Bennett JM, Catovsky D, Daniel MT, Flandrin G, Galton DA, Gralnick HR *et al.* Proposed revised criteria for the classification of acute myeloid leukemia. A report of the French-American-British Cooperative Group. *Ann Intern Med* 1985; **103**: 620–625.
27 Kiyoi H, Naoe T, Nakano Y, Yokota S, Minami S, Miyawaki S *et al.* Prognostic implication of FLT3 and N-RAS gene mutations in acute myeloid leukemia. *Blood* 1999; **93**: 3074–3080.
28 Ozeki K, Kiyoi H, Hirose Y, Iwai M, Ninomiya M, Kodera Y *et al.* Biologic and clinical significance of the FLT3 transcript level in acute myeloid leukemia. *Blood* 2004; **103**: 1901–1908.
29 Yamamoto Y, Kiyoi H, Nakano Y, Suzuki R, Kodera Y, Miyawaki S *et al.* Activating mutation of D835 within the activation loop of FLT3 in human hematologic malignancies. *Blood* 2001; **97**: 2434–2439.
30 Osumi K, Fukui T, Kiyoi H, Kasai M, Kodera Y, Kudo K *et al.* Rapid screening of leukemia fusion transcripts in acute leukemia by real-time PCR. *Leuk Lymphoma* 2002; **43**: 2291–2299.
31 Makishima H, Yoshida K, Nguyen N, Przychodzen B, Sanada M, Okuno Y *et al.* Somatic SETBP1 mutations in myeloid malignancies. *Nat Genet* 2013; **45**: 942–946.
32 Kon A, Shih LY, Minamino M, Sanada M, Shiraishi Y, Nagata Y *et al.* Recurrent mutations in multiple components of the cohesin complex in myeloid neoplasms. *Nat Genet* 2013; **45**: 1232–1237.
33 Sakaguchi H, Okuno Y, Muramatsu H, Yoshida K, Shiraishi Y, Takahashi M *et al.* Exome sequencing identifies secondary mutations of SETBP1 and JAK3 in juvenile myelomonocytic leukemia. *Nat Genet* 2013; **45**: 937–941.
34 Ishikawa Y, Kiyoi H, Tsujimura A, Miyawaki S, Miyazaki Y, Kuriyama K *et al.* Comprehensive analysis of cooperative gene mutations between class I and class II in *de novo* acute myeloid leukemia. *Eur J Haematol* 2009; **83**: 90–98.

35 Speck NA, Gilliland DG. Core-binding factors in haematopoiesis and leukaemia. *Nat Rev Cancer* 2002; **2**: 502–513.
36 Swerdlow S, Campo E, Harris N, Jaffe E, Pileri S, Stein H *et al. WHO Classification of Tumours of Haematopoietic and Lymphoid Tissues*. 4th edn. WHO Press: Lyon, 2008.
37 Vardiman JW, Thiele J, Arber DA, Brunning RD, Borowitz MJ, Porwit A *et al.* The 2008 revision of the World Health Organization (WHO) classification of myeloid neoplasms and acute leukemia: rationale and important changes. *Blood* 2009; **114**: 937–951.
38 Abdel-Wahab O, Levine RL. Mutations in epigenetic modifiers in the pathogenesis and therapy of acute myeloid leukemia. *Blood* 2013; **121**: 3563–3572.
39 Grossmann V, Schnittger S, Kohlmann A, Eder C, Roller A, Dicker F *et al.* A novel hierarchical prognostic model of AML solely based on molecular mutations. *Blood* 2012; **120**: 2963–2972.
40 Cancer Genome Atlas Research N. Genomic and epigenomic landscapes of adult *de novo* acute myeloid leukemia. *N Engl J Med* 2013; **368**: 2059–2074.
41 Tang JL, Hou HA, Chen CY, Liu CY, Chou WC, Tseng MH *et al.* AML1/RUNX1 mutations in 470 adult patients with *de novo* acute myeloid leukemia: prognostic implication and interaction with other gene alterations. *Blood* 2009; **114**: 5352–5361.
42 Stone RM. Acute myeloid leukemia in first remission: to choose transplantation or not? *J Clin Oncol* 2013; **31**: 1262–1266.
43 Paschka P, Schlenk RF, Gaidzik VI, Habdank M, Kronke J, Bullinger L *et al.* IDH1 and IDH2 mutations are frequent genetic alterations in acute myeloid leukemia and confer adverse prognosis in cytogenetically normal acute myeloid leukemia with NPM1 mutation without FLT3 internal tandem duplication. *J Clin Oncol* 2010; **28**: 3636–3643.
44 Dufour A, Schneider F, Metzeler KH, Hoster E, Schneider S, Zellmeier E *et al.* Acute myeloid leukemia with biallelic CEBPA gene mutations and normal karyotype represents a distinct genetic entity associated with a favorable clinical outcome. *J Clin Oncol* 2010; **28**: 570–577.
45 Krzywinski M, Schein J, Birol I, Connors J, Gascoyne R, Horsman D *et al.* Circos: an information aesthetic for comparative genomics. *Genome Res* 2009; **19**: 1639–1645.

Supplementary Information accompanies this paper on the Leukemia website (http://www.nature.com/leu)

Oncogene (2014), 1–9

www.nature.com/onc

ORIGINAL ARTICLE

Rad18 and Rnf8 facilitate homologous recombination by two distinct mechanisms, promoting Rad51 focus formation and suppressing the toxic effect of nonhomologous end joining

S Kobayashi[1], Y Kasaishi[1], S Nakada[2,5], T Takagi[3], S Era[1], A Motegi[1], RK Chiu[4], S Takeda[1] and K Hirota[1,3]

The E2 ubiquitin conjugating enzyme Ubc13 and the E3 ubiquitin ligases Rad18 and Rnf8 promote homologous recombination (HR)-mediated double-strand break (DSB) repair by enhancing polymerization of the Rad51 recombinase at γ-ray-induced DSB sites. To analyze functional interactions between the three enzymes, we created *RAD18*$^{-/-}$, *RNF8*$^{-/-}$, *RAD18*$^{-/-}$/*RNF8*$^{-/-}$ and *UBC13*$^{-/-}$ clones in chicken DT40 cells. To assess the capability of HR, we measured the cellular sensitivity to camptothecin (topoisomerase I poison) and olaparib (poly(ADP ribose)polymerase inhibitor) because these chemotherapeutic agents induce DSBs during DNA replication, which are repaired exclusively by HR. *RAD18*$^{-/-}$, *RNF8*$^{-/-}$ and *RAD18*$^{-/-}$/*RNF8*$^{-/-}$ clones showed very similar levels of hypersensitivity, indicating that Rad18 and Rnf8 operate in the same pathway in the promotion of HR. Although these three mutants show less prominent defects in the formation of Rad51 foci than *UBC13*$^{-/-}$cells, they are more sensitive to camptothecin and olaparib than *UBC13*$^{-/-}$cells. Thus, Rad18 and Rnf8 promote HR-dependent repair in a manner distinct from Ubc13. Remarkably, deletion of Ku70, a protein essential for nonhomologous end joining (NHEJ) significantly restored tolerance of *RAD18*$^{-/-}$ and *RNF8*$^{-/-}$ cells to camptothecin and olaparib without affecting Rad51 focus formation. Thus, in cellular tolerance to the chemotherapeutic agents, the two enzymes collaboratively promote DSB repair by HR by suppressing the toxic effect of NHEJ on HR rather than enhancing Rad51 focus formation. In contrast, following exposure to γ-rays, *RAD18*$^{-/-}$, *RNF8*$^{-/-}$, *RAD18*$^{-/-}$/*RNF8*$^{-/-}$ and *UBC13*$^{-/-}$cells showed close correlation between cellular survival and Rad51 focus formation at DSB sites. In summary, the current study reveals that Rad18 and Rnf8 facilitate HR by two distinct mechanisms: suppression of the toxic effect of NHEJ on HR during DNA replication and the promotion of Rad51 focus formation at radiotherapy-induced DSB sites.

Oncogene advance online publication, 24 November 2014; doi:10.1038/onc.2014.371

INTRODUCTION

Anticancer therapeutic DNA-damaging agents including ionizing radiation, camptothecin (a topoisomerase I poison) and olaparib (an inhibitor against poly(ADP ribose)polymerase) kill cycling cells by inducing double-strand breaks (DSBs). These agents create DSBs in distinct manners, as ionizing radiation generates DSBs in genomic DNA in a higher-order chromatin structure, whereas camptothecin and olaparib generate DSBs in one of the two sister chromatids during DNA replication. Ionizing radiation-induced DSBs are repaired by both homologous recombination (HR) and nonhomologous end joining (NHEJ),[1–4] whereas DSBs induced by camptothecin and olaparib are repaired exclusively by HR.[5–9] The two DSB repair pathways compete with each other as evidenced by the observation that the embryonic mortality caused by a defect in the HR factor BRCA1 is suppressed by the additional mutation of 53BP1, a factor involved in NHEJ.[10]

Vital roles for Rad18 and Rnf8 in genome maintenance have been suggested from a number of studies on cells treated with small interfering RNA (siRNA) for transient depletion of Rad18 or Rnf8. However, the strong effects caused by such transient depletion require careful interpretation as both the *RAD18*$^{-/-}$ and *RNF8*$^{-/-}$ mice develop normally without showing prominent defects in meiotic HR or NHEJ-dependent V(D)J recombination in lymphoid precursors.[11–15] Lack of any prominent phenotype in these mice is partly attributable to difficulty in precise phenotypic analysis of DNA damage response using primary culture cells. Moreover, the acute effect caused by siRNA-mediated transient depletion can be greater than the long-term effect caused by the loss of functional proteins, due to compensation for the loss by upregulation of other proteins in the long term. To analyze the effects caused by the loss of ubiquitylation enzymes involved in DNA damage responses, we have generated isogenic mutants from a single parental cell line, DT40 cells. In addition, to precisely distinguish the catalytic role from the non-ubiquitylation role of Rad18 and Rnf8, we created ubiquitylation-dead mutants (*RAD18*$^{C29F/-}$ and *RNF8*$^{C398F/-}$ cells) as well as null mutants (*RAD18*$^{-/-}$ and *RNF8*$^{-/-}$ cells; Table 1).

In this study, we analyzed the capability of *RAD18*$^{-/-}$, *RNF8*$^{-/-}$, *RAD18*$^{-/-}$/*RNF8*$^{-/-}$ and *UBC13*$^{-/-}$clones to perform HR to repair DSBs, and made the following three conclusions. First, Rad18 and Rnf8 facilitate DSB repair by HR using two distinct mechanisms: promoting Rad51 focus formation at γ-ray-induced DSB sites and

[1]Department of Radiation Genetics, Kyoto University Graduate School of Medicine, Kyoto, Japan; [2]Center of Integrated Medical Research, School of Medicine, Keio University, Tokyo, Japan; [3]Department of Chemistry, Graduate School of Science and Engineering, Tokyo Metropolitan University, Tokyo, Japan and [4]Department of Radiation Oncology, University Medical Center Groningen, University of Groningen, Groningen, The Netherlands. Correspondence: Dr K Hirota or Dr S Takeda, Department of Radiation Genetics, Kyoto University, Graduate School of Medicine, Yoshida Konoe, Sakyo-ku, Kyoto 606-8501, Japan.
E-mail: khirota@rg.med.kyoto-u.ac.jp or stakeda@rg.med.kyoto-u.ac.jp
[5]Current address: Department of Bioregulation and Cellular Response, Graduate School of Medicine, Osaka University, Osaka, Japan.
Received 11 April 2014; revised 25 September 2014; accepted 27 September 2014

Table 1. DT40 mutants used in this study

Cell line	*Selection marker for gene disruption*		*Reference*
	First gene	*Second gene*	
RNF8$^{-/-}$	*bsr/puro*	—	This study
UBC13$^{-/-}$	*bsr/his*	—	16
RAD18$^{-/-}$	*his/hygro*	—	1, 3
RAD18$^{-/-}$/*RNF8*$^{-/-}$	*his/hygro*	*bsr/puro*	This study
KU70$^{-/-}$	*his/bsr*	—	4
RNF8$^{-/-}$/*KU70*$^{-/-}$	*his/bsr*	*puro/neo*	This study
RAD18$^{-/-}$/*KU70*$^{-/-}$	*puro/hygro*	*his/bsr*	3
RNF8$^{C398F/-}$	*bsr*/Cre-excised *puro*	—	This study
RAD18$^{C29F/-}$	*neo*/Cre-excised *puro*	—	This study
RAD18$^{-/-}$/*RNF8*$^{C398F/-}$	*his/hygro*	*bsr*/Cre-excised *puro*	This study
RNF8$^{-/-}$/*RAD18*$^{C29F/-}$	Cre-excised both *bsr* and *puro*	*neo*/Cre-excised *puro*	This study

suppressing the toxic effect of NHEJ on HR during the repair of DSBs induced by camptothecin and olaparib. Second, Rad18 and Rnf8 promote Rad51 focus formation independently of each other, whereas the two enzymes function in the same pathway in suppressing the toxic effect of NHEJ on HR. Third, the non-catalytic functioning of Rad18 and Rnf8 significantly contributes to Rad51 focus formation.

RESULTS

RNF8$^{-/-}$ and *UBC13*$^{-/-}$ cells display distinctly different phenotypes

To disrupt the chicken *RNF8* locus, we constructed two targeting vectors, *RNF8-puro* and *RNF8-bsr* (Supplementary Figure 1A), and sequentially transfected these constructs into wild-type DT40 cells. Targeted disruption of the *RNF8* gene was verified by Southern blot analysis of *Xba*I-digested genomic DNA with the use of an external 3′ probe (Supplementary Figure 1B). Reverse transcription-PCR analysis showed the loss of RNF8 expression confirming disruption of the *RNF8* gene (Supplementary Figure 1C). *RNF8*$^{-/-}$cells proliferated with normal kinetics, whereas *UBC13*$^{-/-}$ cells proliferated with slower kinetics due to spontaneously occurring apoptosis, compared with wild-type cells[16] (Figure 1a). The extent of apoptosis during the cell cycle was closely correlated with the number of spontaneously arising mitotic chromosomal breaks among isogenic DNA repair-deficient DT40 mutants.[17] In agreement with the close correlation, *RNF8*$^{-/-}$ cells exhibited no increase in the number of spontaneous chromosomal breaks, whereas *UBC13*$^{-/-}$ cells exhibit a significant increase (Figure 1b). The severe genome instability of *UBC13*$^{-/-}$ cells agrees with the embryonic lethality of *UBC13*$^{-/-}$ mice.[18,19] These observations indicate that Ubc13 is able to contribute to genome maintenance independently of Rnf8.

To determine in which DNA repair pathways Rnf8 has a role, we measured cellular survival after exposure of cells to DNA-damaging agents. *KU70*$^{-/-}$ cells, but not *RNF8*$^{-/-}$ cells, were sensitive to ICRF193,[20,21] a catalytic inhibitor of topoisomerase II (Figure 1c), indicating that Rnf8 is not involved in the promotion of canonical NHEJ. We then measured sensitivity to camptothecin (a topoisomerase I poison) and olaparib (a poly (ADP ribose) polymerase inhibitor), two chemotherapeutic agents that induce replication fork collapse. The subsequent restart of replication requires HR with the intact sister chromatid.[5–9] *RNF8*$^{-/-}$ cells showed greater sensitivity to both camptothecin and olaparib than *UBC13*$^{-/-}$ cells, and the sensitivity was completely reversed by complementation with a *RNF8* transgene (Supplementary Figures 1D and F). The hypersensitivity in *RNF8*$^{-/-}$ cells to camptothecin is consistent with results of a previous study.[22] From the data of Figures 1d and e, we conclude that Rnf8 can function independently of Ubc13 in the cellular tolerance to the chemotherapeutic agents.

The Rad18 and Rnf8 ubiquitin ligases are compensatory for each other in genome maintenance and promotion of Rad51 polymerization at γ-ray-induced DSB sites

To analyze the functional relationship between Rad18 and Rnf8, we generated *RAD18*$^{-/-}$/*RNF8*$^{-/-}$ double mutant cells. Spontaneously arising chromosome breaks in *RAD18*$^{-/-}$/*RNF8*$^{-/-}$ double mutant were increased fourfold as compared with either *RAD18*$^{-/-}$ or *RNF8*$^{-/-}$ single-mutant cells (Figure 1b). This result reveals substantial functional redundancy between Rad18 and Rnf8 in genome maintenance during the cell cycle.

We next measured the sensitivity of *RAD18*$^{-/-}$/*RNF8*$^{-/-}$ cells to ICRF193, camptothecin, olaparib and γ-rays. *RAD18*$^{-/-}$, *RNF8*$^{-/-}$ and *RAD18*$^{-/-}$/*RNF8*$^{-/-}$ cells showed no sensitivity to ICRF193 (Figure 2a); however, they were similarly sensitive to camptothecin (Figure 2b). Moreover, the three types of cells showed similar sensitivity to olaparib (Figure 2c). In sharp contrast, *RAD18*$^{-/-}$/*RNF8*$^{-/-}$ cells showed significantly greater sensitivity to γ-rays than observed with *RAD18*$^{-/-}$ or *RNF8*$^{-/-}$ cells (Figure 2d). We therefore conclude that Rad18 and Rnf8 ubiquitin ligases operate in the same pathway in the HR-mediated repair of DSBs induced by the two chemotherapeutic agents, whereas Rad18 and Rnf8 can facilitate HR-mediated repair of γ-ray-induced DSBs independently of one another. To explore the role of the two ubiquitin ligases in HR, we measured Rad51 focus formation following γ-rays irradiation. The Rad51 focus formation of *RAD18*$^{-/-}$/*RNF8*$^{-/-}$ cells was reduced 2.5-fold as compared with either *RAD18*$^{-/-}$ or *RNF8*$^{-/-}$ cells (Figure 2e and Supplementary Figure 2B). This phenotype agrees with the γ-ray sensitivity of *RAD18*$^{-/-}$, *RNF8*$^{-/-}$ and *RAD18*$^{-/-}$/*RNF8*$^{-/-}$ cells. Thus, the two ubiquitin ligases independently promote the function of Rad51 at γ-ray-induced DSBs.

To investigate whether the functional redundancy seen in the DT40 clones were relevant to human cells, we analyzed γ-ray-induced Rad51 focus formation in human HCT116 cells. The depletion of Rnf8 was assessed by analyzing the disappearance of 53BP1 foci[23–25] (Supplementary Figure 3). Similar to the observation in *RAD18*$^{-/-}$ mouse embryonic fibroblasts,[26] *RAD18*$^{-/-}$ HCT116 cells displayed only a slight defect in Rad51 focus formation. Although the depletion of Rnf8 caused only a mild reduction of Rad51 foci formation in the *RAD18*$^{+/+}$ HCT116 cells, it significantly decreased the number of Rad51 foci in the *RAD18*$^{-/-}$ cells (Figure 2f and Supplementary Figure 3). We therefore conclude that Rad18 and Rnf8 independently contribute to the Rad51 focus formation at γ-ray-induced DSBs in the chicken and human cells.

The inactivation of NHEJ in *RNF8*$^{-/-}$ and *RAD18*$^{-/-}$ cells significantly restores their tolerance to camptothecin and olaparib

The epistatic relationship between *RAD18* and *RNF8* in cellular tolerance to camptothecin and olaparib (Figures 2b and c) led us to investigate whether Rnf8 suppresses the toxic effect of NHEJ on HR as does Rad18.[3] We inactivated NHEJ by disrupting the *KU70* gene in *RNF8*$^{-/-}$ cells, and found that the loss of Ku70 in *RNF8*$^{-/-}$ as well as *RAD18*$^{-/-}$ cells completely restored their cellular tolerance to camptothecin (Figure 3a). Similarly, *RNF8*$^{-/-}$/*KU70*$^{-/-}$ and *RAD18*$^{-/-}$/*KU70*$^{-/-}$ cells were more tolerant to olaparib than *RAD18*$^{-/-}$ and *RNF8*$^{-/-}$ cells (Figure 3b). Thus, Rad18 and Rnf8 might suppress the toxic effect of NHEJ on HR. To verify that the observed cellular tolerance represents the capability of cells to repair one-end breaks, which occur as a consequence of replication over broken template strands,

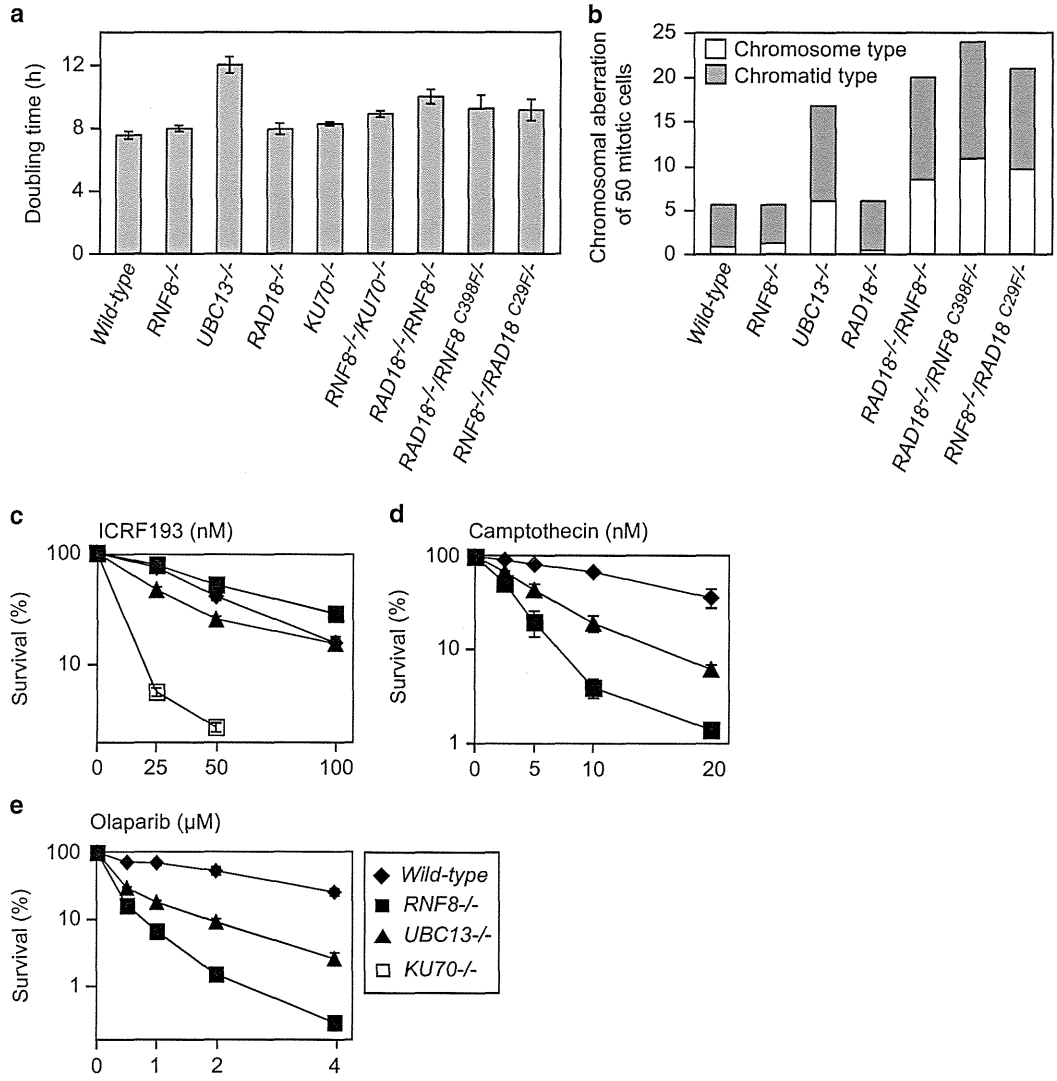

Figure 1. *RNF8*$^{-/-}$ and *UBC13*$^{-/-}$ cells display distinctly different phenotypes. (**a**) The average doubling time for the indicated genotypes. Error bars show the s.e. in at least three independent experiments. (**b**) Spontaneously arising chromosomal aberrations in 50 mitotic cells. Two breaks at the same site of both sister chromatids are defined as chromosome-type breaks (white rectangle), whereas breaks at one of the two sister chromatids are chromatid-type (gray rectangle). (**c**–**e**) Cellular sensitivity to ICRF193 (**c**), camptothecin (**d**) and olaparib (**e**) was analyzed. Survival rate was calculated as the percentage of surviving cells treated with DNA-damaging agents relative to the untreated surviving cells. The concentration or dose is displayed on the horizontal axis on a linear scale, whereas the survival rate is displayed on the *y* axis on a logarithmic scale. Error bars show the s.e. of the mean in at least three independent experiments.

we examined chromosomal aberrations in mitotic cells having been treated with camptothecin. *RNF8*$^{-/-}$ and *RAD18*$^{-/-}$ cells showed significant increases in the number of chromosomal aberrations compared with wild-type cells, whereas such increases were not seen in *RNF8*$^{-/-}$/*KU70*$^{-/-}$ and *RAD18*$^{-/-}$/*KU70*$^{-/-}$ cells (Figure 3c). Thus, cellular survival (Figure 3a) represents the capability of cells to repair one-end breaks. Taken together, we conclude that the collaboration between Rad18 and Rnf8 suppresses the toxic effect of NHEJ on HR-dependent repair of one-end breaks (Figure 3c).

There are three possible mechanisms underlying the toxic effect by NHEJ. The Ku proteins might suppress HR by inhibiting the polymerization of Rad51 at one-end breaks or by interfering with subsequent steps such as homology search and strand exchange. The third mechanism involves aberrant NHEJ of two one-end breaks derived from neighboring stalled replication forks. We measured Rad51 focus formation following exposure of cells to camptothecin, and found that the loss of Ku70 did not restore the Rad51 focus formation of *RNF8*$^{-/-}$ cells (Figure 3d and Supplementary Figure 2A). Thus, Rnf8 suppresses the toxic effect of NHEJ on HR presumably by facilitating homology search and/or strand exchange. To address the third mechanism, we counted the number of radial chromosomes (Figures 3c, e and f), which arises mainly as a consequence of aberrant NHEJ,[10] as NHEJ-deficient *KU70*$^{-/-}$ cells exhibited a few times lower radial chromosomes events when compared with wild-type cells (Figure 3f). The number of radial chromosomes in *RAD18*$^{-/-}$/*RNF8*$^{-/-}$ cells was very similar to that in *RNF8*$^{-/-}$ and *RAD18*$^{-/-}$ cells. Strikingly, the loss of Ku70 in *RNF8*$^{-/-}$ and *RAD18*$^{-/-}$ cells greatly reduced the number of radial chromosomes (Figures 3c and f). We conclude that Rad18 and Rnf8 work together to promote HR-dependent repair of one-end breaks by inhibiting both aberrant NHEJ of two one-end breaks and a suppressive effect of NHEJ on HR.

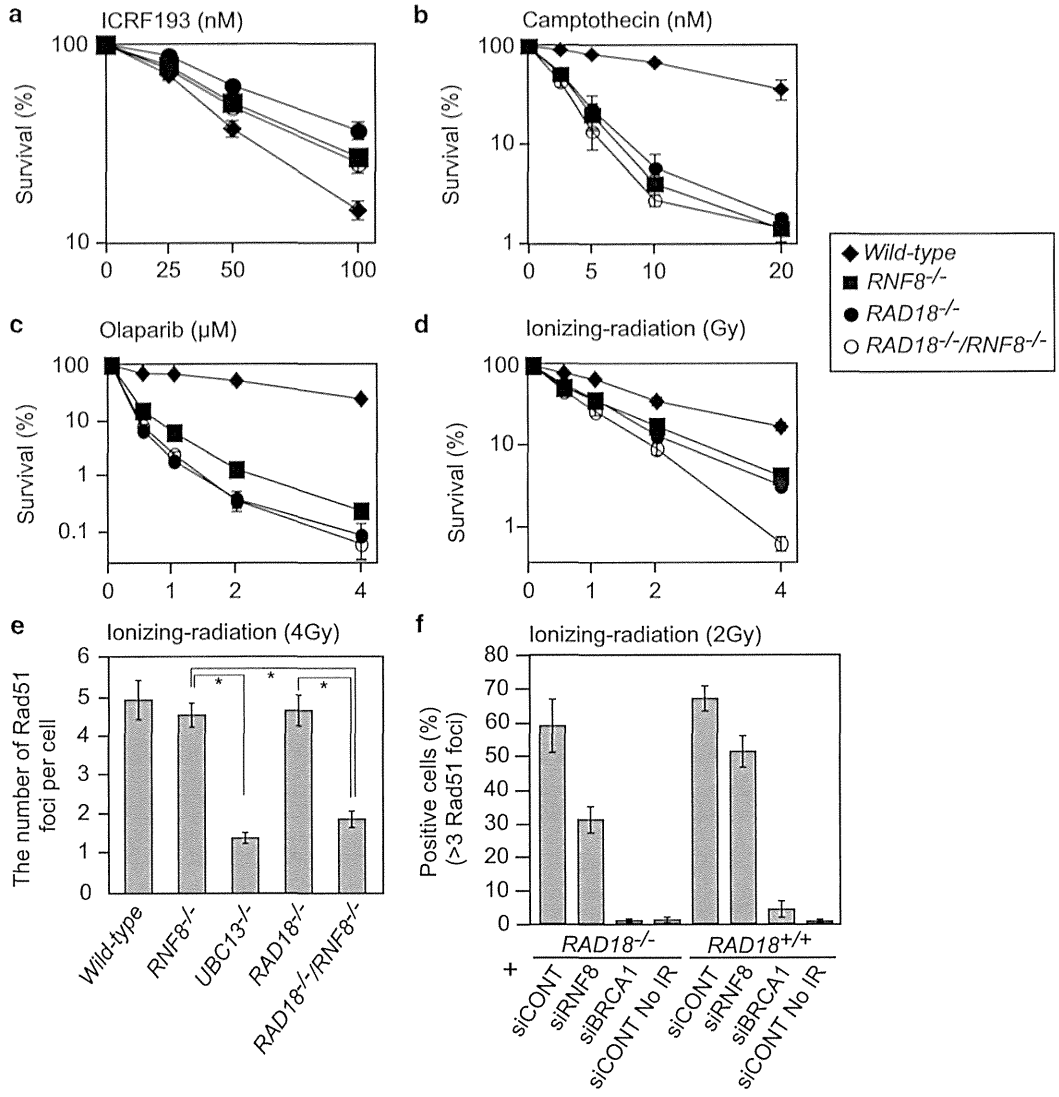

Figure 2. The Rad18 and Rnf8 ubiquitin ligases operate in the same pathway in cellular tolerance to camptothecin and olaparib, whereas they promote Rad51 recruitment to γ-ray-induced DSB sites independently of each other. (**a–d**) Cellular survival of the indicated DNA-damaging agents is shown as in Figure 1. ICRF193 (**a**), camptothecin (**b**), olaparib (**c**) and ionizing radiation (^{137}Cs γ-ray) (**d**). (**e**) The average number of γ-ray-induced Rad51 foci per cell. Cells were fixed 1h after 4 Gy γ-rays irradiation and then stained with anti-Rad51 antibody. Each histogram represents the value obtained by subtracting the number of Rad51 foci in non-irradiated controls from observed foci 1 h after irradiation. The actual number of the number of Rad51 foci is shown in Supplementary Figure 2B. Cells (100–200) were counted and error bars represent s.e. calculated from at least three independent experiments. Statistical significance was determined by a Student's *t*-test: $^{*}P < 0.01$. (**f**) HCT116 cells transfected with the indicated siRNAs were exposed to 2 Gy ionizing radiation. Six hours after irradiation (IR), cells were fixed and subjected to Rad51 and 53BP1 immunofluorescence analysis. Cells treated with siRNA for 2 days were used in this experiment. Depletion of RNF8 was assessed by the disappearance of 53BP1 foci (Supplementary Figure 3). Cells with more than three Rad51 foci were counted as positive cells. Cells (300) were counted. Data are represented as the mean ± s.d. ($n = 3$).

Figure 3. Collaboration between Rad18 and Rnf8 suppresses the toxic effect of NHEJ on HR and contributes to the cellular tolerance to camptothecin and olaparib. (**a**, **b**) Cellular sensitivity to camptothecin (**a**), olaparib (**b**) and γ-rays (**d**) is shown as in Figure 1. Lethal dose 30% (LD30) is the concentration of DNA-damaging agents that reduces cellular survival to 30% relative to cells non-treated with DNA-damaging agents. (**c**) Chromosomal aberrations in cells treated with 10 nM camptothecin. The data represent the mean and s.d. from three independent counts each analyzing 50 mitotic cells. (**d**) The average number of Rad51 foci per cell in camptothecin-treated cells. Cells were exposed to 40 nM camptothecin for 1h and then stained with anti-Rad51 antibody. Each histogram represents the value obtained by subtracting the number of Rad51 foci in non-irradiated controls from observed foci 1h after irradiation. The actual number of Rad51 foci is shown in Supplementary Figures 2A and B. Cells (100–200) were counted in each experiment, and error bars represent s.e. calculated from at least three independent experiments. *P*-value was calculated by a Student's *t*-test: $^{*}P < 0.01$ and NS (not significant). (**e**) Representative images of radial chromosomes are shown. Arrows indicate radial chromosomes. (**f**) Formation of radial chromosomes in cells treated with 100 nM camptothecin. The data represent the mean and s.d. from three independent experiments each analyzing 200 mitotic cells. *P*-value was calculated by a Student's *t*-test: $^{*}P < 0.01$, $^{**}P < 0.05$ and NS (not significant).

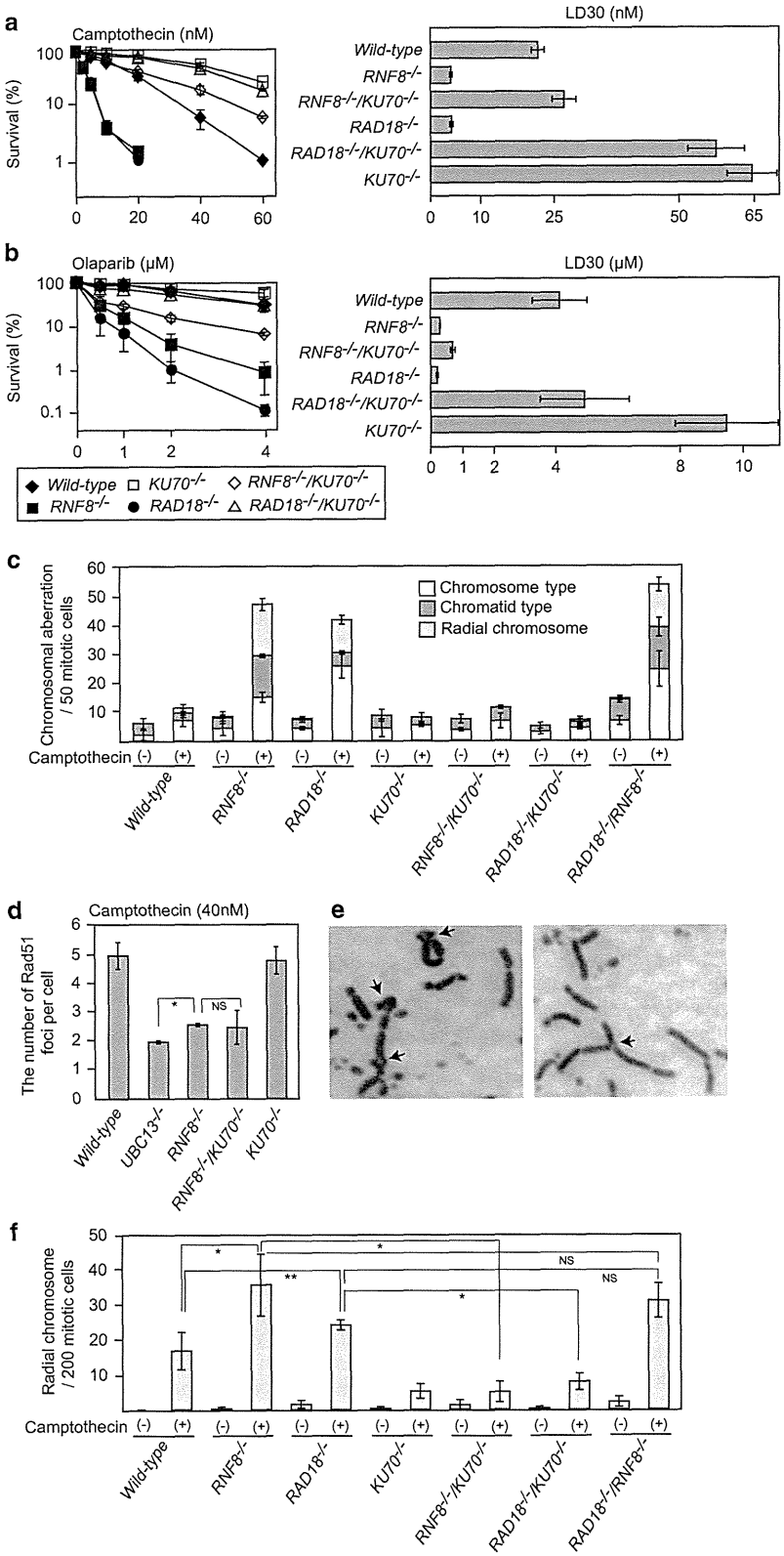

In summary, Rnf8 and Rad18 facilitate HR in two distinctly different ways, the promotion of Rad51 polymerization at DSB sites and suppression of the toxic effect by NHEJ on HR. Moreover, the functional relationship between Rad18 and Rnf8 differs depending on DNA-damaging agents, as the two enzymes are compensatory for each other in the promotion of Rad51 polymerization at γ-ray-induced DSBs, whereas the two enzymes operate in the same pathway in maintaining replication fork progression when cells are exposed to camptothecin and olaparib.

The ubiquitylation activity of Rad18 and Rnf8 is essential for cellular tolerance to camptothecin and olaparib

Accumulating evidence has suggested a non-catalytic (non-ubiquitylation) function of Rad18 and Rnf8 in the initial step of HR-dependent DSB repair.[26–28] To address possible non-ubiquitylation roles of Rad18 and Rnf8, we selectively inactivated the ubiquitylation activity by mutating C398F and C29F in the *RNF8* and *RAD18* genes, respectively,[26,27,29] and generated $RNF8^{C398F/-}$ (Supplementary Figure 4A), $RAD18^{C29F/-}$ (Supplementary Figure 5A), $RAD18^{-/-}/RNF8^{C398F/-}$ and $RNF8^{-/-}/RAD18^{C29F/-}$ clones. The *RNF8* and *RAD18* knock-in mutations were confirmed by reverse transcription-PCR (Supplementary Figures 4B and 5B) and sequence analysis. The C398F mutation completely inactivates the ubiquitylation activity of Rnf8, as $RNF8^{C398F/-}$ as well as $RNF8^{-/-}$ cells showed no ubiquitin foci at γ-ray-induced DSB sites (Supplementary Figure 4C). The C29F mutation also inhibits the ubiquitylation activity of Rad18, as UV-induced monoubiquitylation of proliferating cell nuclear antigen (PCNA) was not increased in $RAD18^{C29F/-}$ or $RAD18^{-/-}$ cells (Supplementary Figure 5C).

We first evaluated the effects of the C29F and C398F mutations on the maintenance of genome integrity (Figure 1b). The number of spontaneously arising mitotic chromosomal breaks in $RNF8^{-/-}/RAD18^{C29F/-}$ and $RAD18^{-/-}/RNF8^{C398F/-}$ clones was very similar to that in $RAD18^{-/-}/RNF8^{-/-}$ cells, indicating that the catalytic functioning of the two enzymes is critical for genome stability. Next we evaluated the effects of the C29F and C398F mutations on the cellular tolerance to camptothecin and olaparib (Figures 4a and b). The C29F and C398F mutations had the same effect on the cellular tolerance to both camptothecin and olaparib, as did the null mutations of the *RAD18* and *RNF8* genes (Figures 4a and b). Therefore, the ubiquitylation activity of both Rad18 and Rnf8 is essential for repressing the toxic effect of NHEJ on HR-dependent DSB repair.

The contribution of non-ubiquitylation roles played by Rad18 and Rnf8 in initiating HR at γ-ray-induced DSB sites

We next evaluated the non-catalytic functions of Rad18 and Rnf8 in the repair of γ-ray-induced DSBs as well as γ-ray-induced Rad51 focus formation. The *RAD18* C29F mutation had the same effect on γ-ray sensitivity as the $RAD18^{-/-}$ null mutation (Figure 4c). Similarly, the *RNF8* C398F mutation had the same effect on γ-ray sensitivity as the $RNF8^{-/-}$ null mutation (Figure 4c). Thus, the non-ubiquitylation roles played by Rad18 and Rnf8 contribute only marginally, if any, to HR-dependent repair of γ-ray-induced DSBs. To assess the role of ubiquitylation by Rnf8 in Rad51 focus formation, we counted the number of Rad51 foci in ionizing irradiation treated $RAD18^{-/-}$, $RAD18^{-/-}/RNF8^{C398F/-}$ and $RAD18^{-/-}/RNF8^{-/-}$ clones after 1 h. The Rad51 focus formation of $RAD18^{-/-}/RNF8^{C398F/-}$ cells was lower than that of $RAD18^{-/-}$ cells while higher than $RAD18^{-/-}/RNF8^{-/-}$ cells (Figure 4d). This result indicates that Rnf8 promotes Rad51 polymerization through both non-catalytic and protein ubiquitylation, as suggested previously,[27] particularly when Rad18 is absent. Similarly, the Rad51 focus formation of $RNF8^{-/-}/RAD18^{C29F/-}$ cells was an intermediate between those of $RNF8^{-/-}$ and $RAD18^{-/-}/RNF8^{-/-}$ clones (Figure 4d and Supplementary Figure 2B), indicating that the non-catalytic function of Rad18 has an important role in Rad51 focus formation.

DISCUSSION

In this study, we demonstrated that Rad18 and Rnf8 facilitate HR by two distinct mechanisms, promotion of Rad51 focus formation and suppression of the toxic effect of NHEJ on HR. The latter mechanism does not require the promotion of Rad51 focus formation as the loss of Ku70 reversed the cellular tolerance of $RNF8^{-/-}$ cells to camptothecin without changing Rad51 focus formation (Figure 3d). Thus, Rad18 and Rnf8 contribute to cellular tolerance to antimalignant therapies with more complex mechanism than previously appreciated.

We also revealed complex functional relationships between the Rad18 and Rnf8 ubiquitin ligases. The two enzymes operate in the same pathway in cellular tolerance to camptothecin and olaparib (Figures 2b and c), whereas they work independently in both cellular tolerance to radiotherapy (Figure 2d) and promoting the function of Rad51 at DSBs induced by γ-rays (Figures 2e and f). Moreover, the catalytic role of Rad18 and Rnf8 is required for the cellular tolerance to camptothecin, olaparib and radiotherapy (Figures 4a–c), whereas the non-catalytic function of both enzymes contributed to Rad51 focus formation (Figure 4d). In summary, the functional relationship between Rad18 and Rnf8 in DNA damage responses is distinctly different depending on the type of DNA damage.

Although a large number of studies previously suggested pivotal roles of Rad18 and Rnf8 in DNA damage responses, mice deficient in either Rad18 or Rnf8 display only modest phenotypes and are capable of performing meiotic HR.[13,30] The moderate phenotypes imply that other related enzymes potentially compensate for the absence of Rad18 or Rnf8. We demonstrated in this study that the two enzymes compensate for one another in the maintenance of chromosomal DNA, as only $RAD18^{-/-}/RNF8^{-/-}$ cells but not $RAD18^{-/-}$ or $RNF8^{-/-}$ cells showed severe genome instability (Figure 1b) as observed in $UBC13^{-/-}$ cells.[16] Conceivably, the dramatic phenotype of $RAD18^{-/-}/RNF8^{-/-}$ and $UBC13^{-/-}$ cells results from combined defects of HR-dependent DSB repair coupled with defects in post-replicational repair. In summary, Rad18 and Rnf8 have a substantially redundant role in genome maintenance.

HR has a dominant role over NHEJ in DSB repair of *Saccharomyces cerevisiae*, whereas HR and NHEJ contribute equally to the whole DSB repair outcome in metazoan cells. Given that in metazoans, a DSB is targeted by both HR and NHEJ, the two pathways could potentially interfere with each other and prevent effective DSB repair (reviewed in Chapman *et al.*[31]). To avoid such interference, NHEJ must be actively inhibited, in particular for the repair of the DSBs that occur in one of the two sister chromatids during DNA replication. This is because camptothecin and olaparib induce numerous DSBs associated with replication and these DSBs are repaired accurately by HR but not by NHEJ. Recent study has reported that the loss of 53BP1 in Brca1-deficient cells rescues HR defect, indicating that Brca1 antagonizes 53BP1 and promotes end resection in S phase.[10] Our current study further revealed that a collaboration between Rad18 and Rnf8 prevent the function of NHEJ and thereby facilitates HR-mediated repair of DSBs induced by camptothecin and olaparib. Moreover, NHEJ causes an increase in the number of radial chromosomes in both $RNF8^{-/-}$ and $RAD18^{-/-}$ cells (Figures 3c and f). We also revealed that the inhibition of NHEJ requires functional ubiquitylation capability of the two enzymes (Figures 4a and b), perhaps monoubiquitylation by Rad18 followed by polyubiquitylation by Rnf8. The precise identity of the Rad18 and Rnf8 ubiquitylation substrate remains an important unresolved question. Although ubiquitylation of 53BP1, Ku80 and proteins involved in the Fanconi anemia pathway by Rad18[32,33] was reported, they might not contribute to cellular

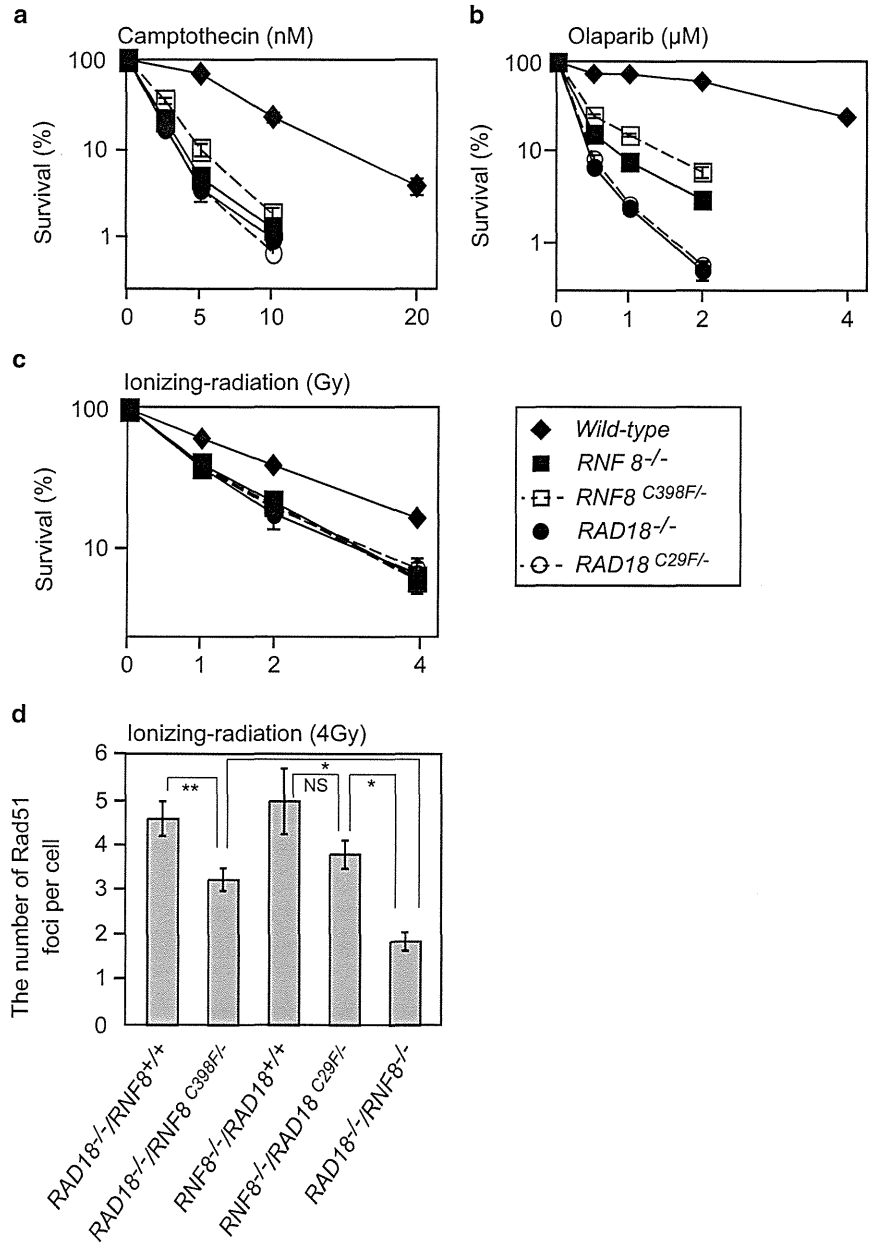

Figure 4. The ubiquitylation activity of Rad18 and Rnf8 is essential for cellular tolerance to camptothecin, olaparib and ionizing radiation. (**a**–**c**) Cellular sensitivity to camptothecin (**a**), olaparib (**b**) and ionizing radiation (**c**) is shown as in Figure 1. Error bars represent the s.e. of the mean in at least three independent experiments. (**d**) The average number of Rad51 foci at 1 h after γ-ray irradiation. More than 100 cells were counted in each experiment and the data represent the mean and s.e. from at least three independent experiments. $*P < 0.01$, $**P < 0.05$ and NS (not significant).

tolerance to camptothecin and olaparib. The rationale for this is because 53BP1 and Ku80 could repress an initial step of HR, whereas Rad18 and Rnf8 inhibit the toxic effect of NHEJ on HR without affecting Rad51 focus formation (Figure 3d). Future studies are required to identify substrates for ubiquitylation as well as the structure of ubiquitylation at various DNA lesions.

MATERIALS AND METHODS

Plasmid construction

For disrupting the *RNF8* gene, *RNF8-puro*, *RNF8-bsr* and *RNF8-neo* were generated from genomic PCR products using the primers 5′-GTA ACTGTAGGCCGGGGATTAGATCTCACG-3′ and 5′-CGGCTCAGTTCTTCC ATCAGAGCATGATGC-3′. Amplified PCR products were cloned into the pCRII-TOPO vector (Invitrogen, Carlsbad, CA, USA). The 5.3-kb *Xba*I fragment from the cloned PCR amplified region was further subcloned into the *Xba*I site of the pBluescriptII KS (+) vector. Each marker gene cassette was ligated into the *Bam*HI site that corresponds to the 86th amino-acid residue of the *RNF8* coding sequence. The 1.2-kb fragment from genomic DNA amplified using the primers 5′-GCATCATGCTCT GATGGAAGAACTGAGCCG-3′ and 5′-GCAATAATGGTGGGAACTGCACATG TGGAG-3′ was used as a probe for Southern blot analysis. The expression of *RNF8* mRNA was detected by reverse transcription-PCR using the primers 5′-GGCGGCATGGCAGCGTGCGGTGCCTCGAG-3′ and 5′-TTA CACTGTTTAGATAACGCAGTAGCTTCC-3′. Each *RAD18* C29F and *RNF8*

C398F knock-in vector was generated from genomic PCR using the following primers.

For *RAD18* C29F,
5′-AGTCAGAAATAAGCGTGGGTGGATATCCGT-3′
5′-GCTGAAGTAATCGAAG***A***AAATCCCACAGC-3′ for left arm,
5′-GCTGTGGGATTT***T***CTTCGATTACTTCAGC-3′
5′-CTGGCAGAACTGAAGCTCTTCACTAGCTC-3′ for right arm.

Amplified PCR products were cloned into pCR-Blunt II-TOPO vector (Invitrogen). The *Eco*RI fragment from this vector was further subcloned into the *Not*I site of the pBluescriptII KS (+) vector. *Not*I site of this vector was used to clone a marker gene (*puro*) cassette.

For *RNF8* C398F,
5′-GGAGTAAAATGGAAAGATGGGGAAGAGAAT-3′
5′-GCTCAGAACAGATTGTG***A***ACTGCAGCTC-3′ for left arm,
5′-GAGCTGCAGT***T***CACAATCTGTTCTGAGC-3′
5′-TTAGATAACGCAGTAGCTTCCATTAT-3′ for right arm.

Amplified PCR products were cloned into pCR-Blunt II-TOPO vector (Invitrogen). *Sca*I site was used to clone a marker gene (*puro*) cassette.

To detect full-length *RNF8* and *RAD18* mRNAs, following primers were used.

For *RNF8*,
5′-ATGGCAGCGTGCGGTGCCTCGAGGCC-3′
5′-TTAGATAACGCAGTAGCTTCCATTAT-3′.

For *RAD18*,
5′-ATGGCCCTGGCGCTGCCCGAACCGC-3′
5′-TCAGCTCTTCTTCCTCTTGCTCCTG-3′.

For the detection of *PCNA* mRNA,
5′-GGGATGTTTGAGGCGCGGCTTGT-3′
5′-CCTCAGTCCCAGTGCAGTTAAGA-3′.

Generation of *RNF8*$^{-/-}$, *RNF8*$^{-/-}$*/KU70*$^{-/-}$, *RAD18*$^{-/-}$*/RNF8*$^{-/-}$, *RAD18* C29F and *RNF8* C398F knock-in mutants

Wild-type DT40 cells were sequentially transfected with the *RNF8-bsr* and the *RNF8-puro* targeting constructs to obtain *RNF8*$^{-/-}$ cells. The gene-targeting frequency of the stably transfected clones was 50% for the *RNF8*$^{-/+}$ cells and 20% for the *RNF8*$^{-/-}$ clones. The *RNF8-puro* and the *RNF8-neo* targeting constructs were sequentially transfected into *KU70*$^{-/-}$ cells to obtain *RNF8*$^{-/-}$*/KU70*$^{-/-}$ cells. *RAD18*$^{-/-}$cells were sequentially transfected with the *RNF8-bsr* and the *RNF8-puro* targeting constructs to obtain *RAD18*$^{-/-}$*/RNF8*$^{-/-}$ cells. The establishment of each mutant was confirmed by Southern blotting. To establish *RAD18* C29F and *RNF8* C398F knock-in mutants, each construct described above was transfected into *RAD18*$^{+/-}$ (and *RNF8*$^{-/-}$*/RAD18*$^{+/-}$) or *RNF8*$^{+/-}$(and *RAD18*$^{-/-}$*/ RNF8*$^{+/-}$), respectively, and then gene targeting was validated by PCR. To remove the resistant gene, cells were transfected with the Cre recombinase expression vector and then treated with 0.2 μM tamoxifen. Forty-eight hours after the treatment, cells were subcloned and puromycin-sensitive clones were selected.

Chromosome aberration analysis

Karyotype analysis was performed as described previously.[34] For the morphological analysis of chromosome aberrations, cells were treated with colcemid for 3 h to enrich for mitotic cells. To count camptothecin-induced chromosomal aberrations, cells were treated with 10 or 100 nM camptothcin for 8h and colcemid was added in the last 3 h.

Measurement of cellular sensitivity to DNA-damaging agents

We measured the amount of ATP in cellular lysates to determine the number of live cells.[35] Cells were treated with each DNA-damaging agent in 1 ml of medium using 24-well plates and incubated at 39.5 °C for 48 h (or 72 h for olaparib). We transferred 100 μl of medium containing the cells to 96-well plates and measured the amount of ATP using CellTiter-Glo (Promega, Madison, WI, USA) according to the manufacturer's instructions. Luminescence was measured by Fluoroskan Ascent FL (Thermo Fisher Scientific Inc., Pittsburgh, PA, USA) or ARVO X5 (Perkin Elmer Inc., Branchburg, NJ, USA).

Immunofluorescent visualization of subnuclear focus formation

The experimental conditions for the immunocytochemical analysis were previously described.[28] Briefly, 30 min for FK2 or 1 h for Rad51 after irradiation with ^{137}Cs γ-ray (4 Gy) or after exposure to camptothecin (40 nM) for 1 h, DT40 cells (7×10^5 cells/ml) were collected on a glass slide using Cytospin3 (Shandon, Pittsburgh, PA, USA). Cells were fixed with 4% formaldehyde for 10 min at room temperature. After blocking with 3% bovine serum albumin/phosphate-buffered saline with Tween-20, the fixed cells were treated with specific antibodies. Visualization of the Rad51 and FK2 foci was performed as previously described, using the anti-Rad51 rabbit polyclonal antibody (Bioacademia Inc., Osaka, Japan) or the mouse FK2 antibody (Nippon Biotest Laboratories, Tokyo, Japan). At least 100 morphologically intact cells were examined.

Human HCT116 cells were grown on coverslips and then washed twice with phosphate-buffered saline before fixation. The cells were fixed with 3% paraformaldehyde and permeabilized with 0.5% Triton-X-100/phosphate-buffered saline. After blocking with 3% goat serum/phosphate-buffered saline, the cells were stained with a Rad51 rabbit polyclonal and a 53BP1 mouse monoclonal antibody (BD Bioscience, San Jose, CA, USA) at 4 °C overnight. For secondary staining, we used a goat Alexa555 anti-rabbit (Invitrogen) and a goat Alexa488 anti-mouse antibody (Invitrogen). The DNA was stained with 4′,6-diamidino-2-phenylindole. The coverslips were mounted with Prolong Gold mounting agent (Invitrogen).

siRNA transfection

The following siRNAs were used in this study: control (MISSION SIC-002, Sigma Genosys, Tokyo, Japan), RNF8 (Thermo Fisher Scientific Inc.) and BRCA1 5′-GGA ACC UGU CUC CAC AAA GTT-3′ (Sigma Genosys). RNA interference transfection for RNF8 and BRCA1 was performed using Lipofectamin RNAiMAX (Invitrogen) in reverse transfection mode.

Western blot analysis of monoubiquitylation of PCNA

For the detection of PCNA monoubiquitylation, 1×10^7 cells were irradiated with 30 J/m^2 UV and lysed 1.5 h post treatment with Laemli sample buffer and 5% 2-ME and then boiled for 5 min followed by ice incubation. The sample (10 μl) was run in an SDS–polyacrylamide electrophoresis gel and then proteins were electroblotted onto a polyvinylidene fluoride membrane. The following antibodies were used: mouse monoclonal PCNA PC10 (Santa Cruz, Santa Cruz, CA, USA) and anti-mouse IgG HRP liked (Santa Cruz). Proteins were visualized by Chemi-Lumi One Super (Nacalai Tesque, Inc., Kyoto, Japan).

CONFLICT OF INTEREST

The authors declare no conflict of interest.

ACKNOWLEDGEMENTS

This work was supported in part by the grants-in-aid program of the Ministry of Education, Sports and Culture of Japan (for ST). We thank Drs Tadahiro Shiomi and Naoko Shiomi (National Institute of Radiological Sciences, Japan) for providing us with the HCT116 *RAD18*$^{-/-}$ and *RAD18*$^{+/+}$ cells and Professor Hitoshi Kurumizaka (Waseda University, Japan) for providing us with the anti-Rad51 antibody. Financial support was provided in part by the Uehara Memorial Foundation, the Naito Foundation, Sumitomo Foundation and Kurata Fundation (for KH).

REFERENCES

1 Yamashita YM, Okada T, Matsusaka T, Sonoda E, Zhao GY, Araki K *et al.* RAD18 and RAD54 cooperatively contribute to maintenance of genomic stability in vertebrate cells. *EMBO J* 2002; **21**: 5558–5566.
2 Yoshimura A, Nishino K, Takezawa J, Tada S, Kobayashi T, Sonoda E *et al.* A novel Rad18 function involved in protection of the vertebrate genome after exposure to camptothecin. *DNA Repair (Amst)* 2006; **5**: 1307–1316.
3 Saberi A, Hochegger H, Szuts D, Lan L, Yasui A, Sale JE *et al.* RAD18 and poly(ADP-ribose) polymerase independently suppress the access of nonhomologous end joining to double-strand breaks and facilitate homologous recombination-mediated repair. *Mol Cell Biol* 2007; **27**: 2562–2571.
4 Takata M, Sasaki MS, Sonoda E, Morrison C, Hashimoto M, Utsumi H *et al.* Homologous recombination and non-homologous end-joining pathways of DNA double-strand break repair have overlapping roles in the maintenance of chromosomal integrity in vertebrate cells. *EMBO J* 1998; **17**: 5497–5508.
5 Pommier Y. Topoisomerase I inhibitors: camptothecins and beyond. *Nat Rev* 2006; **6**: 789–802.
6 Bryant HE, Schultz N, Thomas HD, Parker KM, Flower D, Lopez E *et al.* Specific killing of BRCA2-deficient tumours with inhibitors of poly(ADP-ribose) polymerase. *Nature* 2005; **434**: 913–917.

7 Adachi N, So S, Koyama H. Loss of nonhomologous end joining confers camptothecin resistance in DT40 cells. Implications for the repair of topoisomerase I-mediated DNA damage. *J Biol Chem* 2004; **279**: 37343–37348.
8 Farmer H, McCabe N, Lord CJ, Tutt AN, Johnson DA, Richardson TB *et al.* Targeting the DNA repair defect in BRCA mutant cells as a therapeutic strategy. *Nature* 2005; **434**: 917–921.
9 Hochegger H, Dejsuphong D, Fukushima T, Morrison C, Sonoda E, Schreiber V *et al.* Parp-1 protects homologous recombination from interference by Ku and Ligase IV in vertebrate cells. *EMBO J* 2006; **25**: 1305–1314.
10 Bunting SF, Callen E, Wong N, Chen HT, Polato F, Gunn A *et al.* 53BP1 inhibits homologous recombination in Brca1-deficient cells by blocking resection of DNA breaks. *Cell* 2010; **141**: 243–254.
11 Li L, Halaby MJ, Hakem A, Cardoso R, El Ghamrasni S, Harding S *et al.* Rnf8 deficiency impairs class switch recombination, spermatogenesis, and genomic integrity and predisposes for cancer. *J Exp Med* 2010; **207**: 983–997.
12 Santos MA, Huen MS, Jankovic M, Chen HT, Lopez-Contreras AJ, Klein IA *et al.* Class switching and meiotic defects in mice lacking the E3 ubiquitin ligase RNF8. *J Exp Med* 2010; **207**: 973–981.
13 Lu LY, Wu J, Ye L, Gavrilina GB, Saunders TL, Yu X. RNF8-dependent histone modifications regulate nucleosome removal during spermatogenesis. *Dev Cell* 2010; **18**: 371–384.
14 Sun J, Yomogida K, Sakao S, Yamamoto H, Yoshida K, Watanabe K *et al.* Rad18 is required for long-term maintenance of spermatogenesis in mouse testes. *Mech Dev* 2009; **126**: 173–183.
15 Wu J, Chen Y, Lu LY, Wu Y, Paulsen MT, Ljungman M *et al.* Chfr and RNF8 synergistically regulate ATM activation. *Nat Struct Mol Biol* 2011; **18**: 761–768.
16 Zhao GY, Sonoda E, Barber LJ, Oka H, Murakawa Y, Yamada K *et al.* A critical role for the ubiquitin-conjugating enzyme Ubc13 in initiating homologous recombination. *Mol Cell* 2007; **25**: 663–675.
17 Yamazoe M, Sonoda E, Hochegger H, Takeda S. Reverse genetic studies of the DNA damage response in the chicken B lymphocyte line DT40. *DNA Repair (Amst)* 2004; **3**: 1175–1185.
18 Yamamoto M, Okamoto T, Takeda K, Sato S, Sanjo H, Uematsu S *et al.* Key function for the Ubc13 E2 ubiquitin-conjugating enzyme in immune receptor signaling. *Nat Immunol* 2006; **7**: 962–970.
19 Fukushima T, Matsuzawa S, Kress CL, Bruey JM, Krajewska M, Lefebvre S *et al.* Ubiquitin-conjugating enzyme Ubc13 is a critical component of TNF receptor-associated factor (TRAF)-mediated inflammatory responses. *Proc Natl Acad Sci USA* 2007; **104**: 6371–6376.
20 Adachi N, Suzuki H, Iiizumi S, Koyama H. Hypersensitivity of nonhomologous DNA end-joining mutants to VP-16 and ICRF-193: implications for the repair of topoisomerase II-mediated DNA damage. *J Biol Chem* 2003; **278**: 35897–35902.
21 Maede Y, Shimizu H, Fukushima T, Kogame T, Nakamura T, Miki T *et al.* Differential and common DNA repair pathways for topoisomerase I- and II-targeted drugs in a genetic DT40 repair cell screen panel. *Mol Cancer Ther* 2014; **13**: 214–220.
22 Oestergaard VH, Pentzold C, Pedersen RT, Iosif S, Alpi A, Bekker-Jensen S *et al.* RNF8 and RNF168 but not HERC2 are required for DNA damage-induced ubiquitylation in chicken DT40 cells. *DNA Repair (Amst)* 2012; **11**: 892–905.
23 Mailand N, Bekker-Jensen S, Faustrup H, Melander F, Bartek J, Lukas C *et al.* RNF8 ubiquitylates histones at DNA double-strand breaks and promotes assembly of repair proteins. *Cell* 2007; **131**: 887–900.
24 Kolas NK, Chapman JR, Nakada S, Ylanko J, Chahwan R, Sweeney FD *et al.* Orchestration of the DNA-damage response by the RNF8 ubiquitin ligase. *Science* 2007; **318**: 1637–1640.
25 Huen MS, Grant R, Manke I, Minn K, Yu X, Yaffe MB *et al.* RNF8 transduces the DNA-damage signal via histone ubiquitylation and checkpoint protein assembly. *Cell* 2007; **131**: 901–914.
26 Huang J, Huen MS, Kim H, Leung CC, Glover JN, Yu X *et al.* RAD18 transmits DNA damage signalling to elicit homologous recombination repair. *Nat Cell Biol* 2009; **11**: 592–603.
27 Luijsterburg MS, Acs K, Ackermann L, Wiegant WW, Bekker-Jensen S, Larsen DH *et al.* A new non-catalytic role for ubiquitin ligase RNF8 in unfolding higher-order chromatin structure. *EMBO J* 2012; **31**: 2511–2527.
28 Takata M, Sasaki MS, Tachiiri S, Fukushima T, Sonoda E, Schild D *et al.* Chromosome instability and defective recombinational repair in knockout mutants of the five Rad51 paralogs. *Mol Cell Biol* 2001; **21**: 2858–2866.
29 Lu CS, Truong LN, Aslanian A, Shi LZ, Li Y, Hwang PY *et al.* The RING finger protein RNF8 ubiquitinates Nbs1 to promote DNA double-strand break repair by homologous recombination. *J Biol Chem* 2012; **287**: 43984–43994.
30 Inagaki A, van Cappellen WA, van der Laan R, Houtsmuller AB, Hoeijmakers JH, Grootegoed JA *et al.* Dynamic localization of human RAD18 during the cell cycle and a functional connection with DNA double-strand break repair. *DNA Repair (Amst)* 2009; **8**: 190–201.
31 Chapman JR, Taylor MR, Boulton SJ. Playing the end game: DNA double-strand break repair pathway choice. *Mol Cell* 2012; **47**: 497–510.
32 Watanabe K, Iwabuchi K, Sun J, Tsuji Y, Tani T, Tokunaga K *et al.* RAD18 promotes DNA double-strand break repair during G1 phase through chromatin retention of 53BP1. *Nucleic Acids Res* 2009; **37**: 2176–2193.
33 Palle K, Vaziri C. Rad18 E3 ubiquitin ligase activity mediates Fan coni anemia pathway activation and cell survival following DNA Topoisomerase 1 inhibition. *Cell Cycle* 2011; **10**: 1625–1638.
34 Sonoda E, Sasaki MS, Buerstedde JM, Bezzubova O, Shinohara A, Ogawa H *et al.* Rad51-deficient vertebrate cells accumulate chromosomal breaks prior to cell death. *EMBO J* 1998; **17**: 598–608.
35 Ji K, Kogame T, Choi K, Wang X, Lee J, Taniguchi Y *et al.* A novel approach using DNA-repair-deficient chicken DT40 cell lines for screening and characterizing the genotoxicity of environmental contaminants. *Environ Health Perspect* 2009; **117**: 1737–1744.

Supplementary Information accompanies this paper on the Oncogene website (http://www.nature.com/onc)

厚生労働科学研究委託費　難治性疾患等克服研究事業
ゲノム不安定性を示す難治性遺伝性疾患群の症例収集と
ゲノム・分子機能解析による病態解明研究

平成２６年度　委託業務成果報告書

発行　平成２７年３月
発行所　ゲノム不安定性を示す難治性遺伝性疾患群の症例収集とゲノム・分子機能解析による病態解明研究班事務局
〒852-8523　長崎県長崎市坂本 1-12-4
長崎大学原爆後障害医療研究所　原研修復内
TEL 095-819-7102, FAX 095-819-7175